The Astronomical Journal, 127:2997–3017, 2004 May
© 2004. The American Astronomical Society. All rights reserved. Printed in U.S.A.

THE STRANGE CASE OF 133P/ELST-PIZARRO: A COMET AMONG THE ASTEROIDS[1]

Henry H. Hsieh, David C. Jewitt, and Yanga R. Fernández
Institute for Astronomy, University of Hawaii, 2680 Woodlawn Drive, Honolulu, HI 96822; hsieh@ifa.hawaii.edu, jewitt@ifa.hawaii.edu, yan@ifa.hawaii.edu
Received 2003 August 7; accepted 2004 January 20

ABSTRACT

We present a new investigation of the comet-asteroid transition object 133P/(7968) Elst-Pizarro. We find mean optical colors ($B-V = 0.69 \pm 0.02$, $V-R = 0.42 \pm 0.03$, $R-I = 0.27 \pm 0.03$) and a phase-darkening coefficient ($\beta = 0.044 \pm 0.007$ mag deg^{-1}) that are comparable both to other comet nuclei and to C-type asteroids. As in 1996, when this object's comet-like activity was first noted, data from 2002 show a long, narrow dust trail in the projected orbit of the object. Observations over several months reveal changes in the structure and brightness of this trail, showing that it is actively generated over long periods of time. Finson-Probstein modeling is used to constrain the parameters of the dust trail. We find optically dominant dust particle sizes of $a_d \sim 10$ μm released with low ejection velocities ($v_g \approx 1.5$ m s^{-1}) over a period of activity lasting at least 5 months in 2002. The double-peaked light curve of the nucleus indicates an aspherical shape (axis ratio $a/b \geq 1.45 \pm 0.07$) and rapid rotation (period $P_{\rm rot} = 3.471 \pm 0.001$ hr). The practical identification of 133P/Elst-Pizarro as a comet (i.e., a mass-losing body) is not in doubt, but the origin of the mass loss is unclear. The 1996 trail has been previously explained as debris released by a chance impact, but our discovery of recurrent activity renders this interpretation implausible. We consider two hypotheses for the activity in 133P/Elst-Pizarro. The ejection of particles is naturally explained if the object is a barely active Jupiter-family comet that has evolved into an asteroid-like orbit, perhaps under the prolonged action of nongravitational forces due to asymmetric mass loss. In this case, the orbital similarity to the Themis family must be considered coincidental. Alternatively, 133P/Elst-Pizarro could be a true member of the Themis family on which buried ice has been recently excavated by impact.

Key words: comets: general — comets: individual (133P/Elst-Pizarro) — minor planets, asteroids — solar system: general

1. INTRODUCTION

Observationally, the distinction between comets and asteroids is simple: comets show comae (gravitationally unbound atmospheres) and tails, while asteroids do not. The corresponding physical distinction is that comets contain volatile material (e.g., water ice) while asteroids do not. Practically, however, determining whether an object possesses a coma can be challenging and is dependent on observational conditions such as seeing and instrument sensitivity. Faint coma from weak outgassing may easily be missed, blurring the observational distinction between these objects. Hartmann, Tholen, & Cruikshank (1987) described "pristine," "dormant," and "extinct" phases during which an evolving comet would not exhibit cometary activity. Some cometary (volatile-containing) objects might thus be misidentified as asteroids, either because low-level outgassing has been missed or because they are in an inactive phase in which outgassing is actually absent. Historically, much discussion of the inactive-comet problem has been focused on near-Earth asteroids, among which dormant and extinct cometary nuclei might lurk. A poor understanding of the precise effects of nongravitational forces on the long-term dynamical evolution of such bodies results in uncertain knowledge of the fraction of inactive Jupiter-family comets (JFCs) among bona fide asteroids in the near-Earth population. Recent estimates range from $\leq 20\%$ (Fernández, Gallardo, & Brunini 2002; Bottke et al. 2002) to as high as 50% (Harris & Bailey 1998).

Independently of physical characteristics, it should be possible to distinguish comets from asteroids by their dynamical properties. The Tisserand parameter, $T_{\rm J}$, an invariant of motion in the restricted three-body problem, is a commonly used dynamical measure for distinguishing between comets and asteroids. Most JFCs (as well as Halley-family comets, or HFCs), have $T_{\rm J} < 3$, while most main-belt asteroids have $T_{\rm J} > 3$ (Vaghi 1973; Kresák 1980). The case for using $T_{\rm J}$ to identify possible inactive comets was strengthened by Fernández, Jewitt, & Sheppard (2001). They found that nine of 10 (90%) asteroidal objects with $T_{\rm J} < 3$ have dark, comet-like albedos ($\sim$0.02–0.12), compared with only two of 38 (5%) objects with $T_{\rm J} > 3$. This result is compatible with a majority of $T_{\rm J} < 3$ objects being inactive comets. As of 2003 December, about 270 low-Tisserand ($T_{\rm J} < 3$) asteroidal (apparently inactive) objects have been identified. Some of these objects are possible extinct or dormant comets for which detailed physical observations are lacking. Only a few have been searched for evidence of cometary activity in the form of very weak comae, most without success (Luu & Jewitt 1992b).

More troublesome are the few objects with asteroid-like ($T_{\rm J} > 3$) dynamical properties but comet-like physical properties. The least-disputed example is comet 2P/Encke ($T_{\rm J} = 3.03$). Comet 107P/Wilson-Harrington ($T_{\rm J} = 3.09$) has displayed activity only once, in 1949 (Bowell et al. 1992; Fernández et al. 1997). Asteroid 3200 Phaethon ($T_{\rm J} = 4.18$) is the likely parent of the Geminid meteor shower (Williams & Wu 1993) and so has a cometary association, although no coma has been detected. The problem specific to these $T_{\rm J} > 3$

[1] Some of the data presented herein were obtained at the W. M. Keck Observatory, which is operated as a scientific partnership among the California Institute of Technology, the University of California, and the National Aeronautics and Space Administration. The Observatory was made possible by the generous financial support of the W. M. Keck Foundation.

TABLE 1
SELECTION OF PAST OBSERVATIONS OF 133P/ELST-PIZARRO

UT Date	Telescope	Ref.[a]	Moon[b]	Mag.[c]	R[d]	Δ[e]	α[f]	α_{pl}[g]	Det.[h]
1979 Jul 24	Siding Spring 1.2 m	1	N	18.5	2.62	1.62	1.5	−0.6	No
1985 Sep 15	Siding Spring 1.2 m	1	N+1	19	2.78	1.78	3.1	0.2	No
1996 Jul 14	ESO 1.0 m	2	N−1	18.3	2.65	1.77	13.1	−0.6	Yes
1996 Aug 9	ESO 1.0 m	2	N−5	18.0	2.67	1.66	2.9	−0.3	Yes
1996 Aug 21	Klet 0.57 m	2	N+7	17.1	2.68	1.67	2.4	−0.2	Yes
	Cloudcroft 0.6 m	2	N+7	18.2, 18.5	2.68	1.67	2.4	−0.2	Yes
1996 Sep 18	Apache Point 3.5 m	3	N+6	...	2.71	1.84	13.1	0.2	Yes
1997 Oct 1	ESO 2.2 m	4	N	20.9 (R)	3.27	2.63	13.9	0.3	No
1997 Oct 3	Cloudcroft 0.6 m	4	N+2	20.4, 21.1	3.27	2.53	13.4	0.3	No
1997 Oct 4	Cloudcroft 0.6 m	4	N+3	19.3, 19.5	3.27	2.52	13.2	0.3	No

[a] (1) McNaught et al. 1996; (2) Elst et al. 1996; (3) Hammergren 1996 (no magnitude available, though trail was reported); (4) Offutt et al. 1997.
[b] Lunar phase expressed in offset from new Moon ("N") in days.
[c] Reported apparent magnitude. Unless otherwise specified, filter band for magnitude values is photographic.
[d] Heliocentric distance in AU.
[e] Geocentric distance in AU.
[f] Phase angle (Sun-EP-Earth) in degrees.
[g] Orbit-plane angle (between observer and object orbit plane as seen from object) in degrees.
[h] Indication whether detection of a dust trail was reported.

objects is that while comets might *stop* outgassing at times and thus masquerade as inactive, asteroidal objects in cometary orbits, asteroids should not be able to *begin* outgassing, since they ostensibly contain no volatiles to outgas.

In this paper, we present and discuss physical observations of 133P/Elst-Pizarro (hereafter EP), which has an asteroid-like $T_J = 3.16$ and orbits in the outer main asteroid belt. The Themis asteroid family, of which EP is thought to be a member (Tóth 2000), is identified by orbital semimajor axes ranging from $a = 3.047$ AU to $a = 3.220$ AU, eccentricities from $e = 0.119$ to $e = 0.191$, and inclinations from $\sin i = 0.012$ to $\sin i = 0.039$ (Zappalà et al. 1990). Dynamically, EP fits well in this family, with orbital elements $a = 3.16$ AU, $e = 0.17$, and $\sin i = 0.024$.

Past observations of EP are summarized in Table 1. The cometary nature of EP was first discovered on 1996 August 7, when a linear dust feature was observed trailing the object (Elst et al. 1996). Subsequent observations over the next month confirmed the presence of a narrow, structureless cometary dust tail more than 3′ long extending from a point-source–like nucleus with no evident coma. During this time, Elst et al. (1996) reported visual magnitudes for the nucleus ranging from $m = 17.1$ to $m = 18.5$. Marsden (1996) designated the object comet P/1996 N2 (later 133P/Elst-Pizarro and 7968 Elst-Pizarro), correlating it with the asteroidal object 1979 OW_7. The latter had been last observed at magnitudes ranging from $m = 18.5$ to $m = 19.5$ in 1979 at Siding Spring and Palomar, exhibiting no apparent cometary activity (Marsden 1996; McNaught et al. 1996). Another prediscovery report by McNaught et al. (1996) also reported that EP was a point source with a magnitude $m \sim 19$ on 1985 September 15. In 1997, EP again appeared completely point-source–like with no apparent dust trail in observations with the 0.6 m telescope at Cloudcroft or with the 2.2 m reflector at La Silla (Offutt, Marsden, & Boehnardt 1997).

Shortly following the initial dust-trail discovery, Sekanina argued that the trail's antisolar direction and featureless structure suggested an origin from a past dust-emission event, likely occurring between late May and early July of 1996, or 40–80 days past perihelion (Pravec & Sekanina 1996). Later modeling placed particle sizes at micron or submicron scales and also suggested that the dust had been released over the course of several weeks or months prior to discovery, a conclusion inconsistent with the dust emission's being due to a single instantaneous impact event (Boehnhardt et al. 1996).

In an effort to explain EP's mysterious comet-like behavior, Boehnhardt et al. (1998) proposed that EP's surface could contain a component of "icy dirt" that was disturbed and activated by a recent impact. They did not indicate in detail, however, how such volatile material could survive over gigayear timescales in a main-belt object such as EP. Rejecting volatile-driven hypotheses for EP's activity entirely, Tóth (2000) proposed that the 1996 dust production might have resulted from impacts onto EP by a cloud of debris from nearby field asteroid 427 Galene. Specifically, Tóth indicated two possibilities: (1) that outbursts from multiple, successive impacts from 427 Galene's debris cloud created the illusion of continuous, prolonged outgassing, or (2) that a single major impact seismically excited the object such that dust grains (including ejecta material) continued to lift off the surface long after the initial impact.

In our new observations of EP, we witnessed the return of its dust trail. This result reopens the debate over the nature of EP's dust-emission activity and EP itself.

2. OBSERVATIONS

We observed EP between 2002 August and December using a Tektronix 2048 × 2048 pixel CCD at the f/10 focus of the University of Hawaii (UH) 2.2 m telescope on Mauna Kea. The image scale at this focus was 0.″219 pixel^{-1}, which provided better than Nyquist sampling of images in typical seeing from 0.″6 to 1.″2, full width at half-maximum (FWHM). Images were obtained through broadband filters approximating the Kron-Cousins photometric system. Follow-up observations were performed in 2003 September with the 10 m Keck I Telescope on Mauna Kea using the LRIS imaging camera (Oke et al. 1995), which incorporated a Tektronix 2048 × 2048 pixel CCD with an image scale of 0.″215 pixel^{-1}. All observations are summarized in Table 2.

We performed standard image preparation (bias subtraction and flat-field reduction) on all data. Flat fields for UH 2.2 m data were constructed from nightly dithered images of the

TABLE 2
NEW OBSERVATIONS OF 133P/ELST-PIZARRO

UT Date	Weather	Moon[a]	Seeing[b]	N[c]	t[d]	Filters	R[e]	Δ[f]	α[g]	α_{pl}[h]
2002 Aug 19	Cirrus	N+11	1.1	6	2500	*R*	2.857	2.050	14.50	−0.2
2002 Sep 7	Clear	N	0.8	14	4200	*R*	2.886	1.935	8.15	0.1
2002 Sep 8	Clear	N+1	0.8	6	1800	*R*	2.887	1.932	7.78	0.1
2002 Sep 9	Cirrus	N+2	1.2	14	4200	*BVRI*	2.888	1.930	7.55	0.1
2002 Nov 5	Clear	N	0.6	5	1500	*R*	2.977	2.181	13.32	0.6
2002 Nov 6	Clear	N+1	0.9	5	1500	*R*	2.979	2.193	13.57	0.6
2002 Nov 7	Clear	N+2	0.9	4	1200	*R*	2.980	2.205	13.82	0.6
2002 Dec 27	Clear	N−7	1.1	20	6000	*BVRI*	3.061	2.933	18.73	0.4
2002 Dec 28	Clear	N−6	1.2	11	3300	*BVRI*	3.062	2.950	18.71	0.4
2003 Sep 22	Clear	N−4	0.6	9	900	*BVR*	3.457	3.194	16.77	0.1

NOTE.—All 2002 observations were made using the University of Hawaii 2.2 m telescope. The 2003 September observations were made using the 10 m Keck I Telescope. A dust trail is detected in all 2002 observations but not in 2003 September observations.

[a] Phase of the Moon expressed in offset from new Moon ("N") in days.
[b] Approximate average seeing (FWHM) in arcseconds.
[c] Number of images.
[d] Total effective exposure time in seconds.
[e] Heliocentric distance in AU.
[f] Geocentric distance in AU.
[g] Phase angle (Sun-EP-Earth) in degrees.
[h] Orbit-plane angle (between observer and object orbit plane as seen from object) in degrees.

twilight sky. Flat fields for Keck data were constructed from nightly images of the illuminated interior of the telescope dome. Photometry on standard stars and field stars was performed by measuring net fluxes contained within circular apertures with optimum sizes determined from curve-of-growth analysis and dependent on the nightly seeing. The sky background to be subtracted was determined from the median pixel value within a circular annulus surrounding each central aperture.

For photometric measurements of the comet, sky background statistics were measured manually at several points at some distance away from the comet to avoid confusing sky background flux with dust-trail flux. These points were chosen far enough away to avoid dust contamination but close enough to minimize possible effects from residual detector nonuniformities and structure in the background sky. The photometry was then calibrated to Landolt (1992) standard stars to produce absolute photometry for the comet. Several field stars (15–20) were also measured in each comet image to verify the stability of extinction throughout each night.

Measured magnitudes of the nucleus of EP are listed in Tables 3 and 4. Errors are estimates based on uncertainties both in the initial photometric measurements and in standard-star color and air-mass extinction fits. They should be taken as lower limits to the true photometric uncertainties.

Table 5 lists $B-V$, $V-R$, and $R-I$ colors computed from 2002 September, 2002 December, and 2003 September data. As a result of EP's rapid rotation and large photometric range, the nucleus changed brightness significantly in the time between exposures in different filters. Thus, color values listed are computed from interpolated R-band magnitudes estimated from data in Tables 3 and 4 and the resulting composite light curve (to be discussed in the following section). We find weighted mean colors $B-V = 0.69 \pm 0.02$, $V-R = 0.41 \pm 0.03$, and $R-I = 0.27 \pm 0.03$, where the listed uncertainties are errors on the mean of measured magnitudes, averaged in flux space. Mean EP colors are comparable to solar values ($B-V = +0.67$, $V-R = +0.36$, $R-I = +0.35$; Hartmann, Cruikshank, & Degewij 1982; Hartmann et al. 1990) and also to the largely neutral spectra of other C-type Themis-family asteroids (Zellner, Tholen, & Tedesco 1985). The average color of a sample of 12 well-measured cometary nuclei was determined by Jewitt (2002) to be $V-R = 0.45 \pm 0.02$, with minimum and maximum values $V-R = 0.31 \pm 0.02$ and $V-R = 0.58 \pm 0.02$, respectively. Thus, the colors we find for EP are also consistent with those measured for other comets.

3. THE NUCLEUS

3.1. *Rotation and Size*

In order to meaningfully compare observations from different months, we need to remove the effects of varying heliocentric distance R, geocentric distance Δ, and phase angle α (the angle between Earth and the Sun, as viewed from EP). To accomplish this, we normalize the apparent magnitudes, $m_R(R, \Delta, \alpha)$, to $R = \Delta = 1$ AU via

$$m_R(1, 1, \alpha) = m_R(R, \Delta, \alpha) - 5 \log R\Delta, \quad (1)$$

where $m_R(1, 1, \alpha)$ is the reduced magnitude.

Throughout our 2002 observing campaign, EP was in a phase-angle range in which phase functions (magnitude vs. phase angle) for comets and asteroids have been found to be nearly linear. In this regime, the phase function is characterized by a linear phase-darkening coefficient, β, measured in magnitudes per degree of phase angle.

Using a χ^2 minimization linear regression algorithm from Press et al. (1992), we fitted rotationally averaged magnitudes (midpoints of nightly light curves in magnitude space) from each 2002 observing run (see Table 6) to the linear phase function

$$m_R(1, 1, 0) = m_R(1, 1, \alpha) - \beta\alpha \quad (2)$$

to derive the absolute magnitude, $m_R(1, 1, 0) = 15.61 \pm 0.01$ mag, and the linear phase-darkening coefficient, $\beta = 0.044 \pm 0.007$ mag deg^{-1}. This phase coefficient is comparable to values measured for the nuclei of comets P/Tempel 2 ($\beta = 0.035 \pm 0.005$ mag deg^{-1}; Jewitt & Luu 1989), P/Neujmin 1 ($\beta = 0.025 \pm 0.006$ mag deg^{-1}; Delahodde et al. 2001), and 143P/Kowal-Mrkos ($\beta = 0.043 \pm 0.014$ mag deg^{-1}; Jewitt,

TABLE 3

2002 Nucleus Photometry for 133P/Elst-Pizarro

UT Date	JD (2,450,000+)	Filter	Observed Magnitude[a]	Absolute Magnitude[b]
2002 Aug 19	2506.0098	*R*	19.862 ± 0.047	15.386 ± 0.048
	2506.0122	*R*	19.911 ± 0.045	15.435 ± 0.046
	2506.0176	*R*	19.979 ± 0.062	15.503 ± 0.062
	2506.0498	*R*	20.131 ± 0.018	15.655 ± 0.019
	2506.0588	*R*	20.040 ± 0.016	15.564 ± 0.017
2002 Sep 7	2506.1318	*R*	19.992 ± 0.024	15.516 ± 0.025
	2525.0330	*R*	19.623 ± 0.015	15.529 ± 0.017
	2525.0376	*R*	19.661 ± 0.015	15.567 ± 0.017
	2525.0437	*R*	19.767 ± 0.017	15.673 ± 0.018
	2525.0486	*R*	19.867 ± 0.019	15.773 ± 0.020
	2525.0532	*R*	19.841 ± 0.018	15.747 ± 0.019
	2525.0581	*R*	19.828 ± 0.018	15.734 ± 0.019
	2525.0630	*R*	19.765 ± 0.017	15.671 ± 0.018
	2525.0676	*R*	19.764 ± 0.017	15.670 ± 0.018
	2525.0725	*R*	19.676 ± 0.016	15.582 ± 0.017
	2525.0774	*R*	19.650 ± 0.015	15.556 ± 0.017
	2525.0820	*R*	19.635 ± 0.015	15.541 ± 0.017
	2525.0869	*R*	19.599 ± 0.015	15.505 ± 0.017
	2525.0918	*R*	19.568 ± 0.014	15.474 ± 0.016
2002 Sep 8	2525.1165	*R*	19.734 ± 0.017	15.640 ± 0.018
	2525.9062	*R*	19.652 ± 0.020	15.578 ± 0.021
	2525.9116	*R*	19.741 ± 0.020	15.667 ± 0.021
	2526.0227	*R*	19.615 ± 0.022	15.541 ± 0.023
	2526.0276	*R*	19.556 ± 0.019	15.482 ± 0.020
	2526.0635	*R*	19.832 ± 0.022	15.758 ± 0.023
2002 Sep 9	2526.0681	*R*	19.822 ± 0.022	15.748 ± 0.023
	2526.8713	*R*	19.753 ± 0.018	15.690 ± 0.019
	2526.8765	*R*	19.730 ± 0.018	15.667 ± 0.019
	2526.8816	*R*	19.669 ± 0.017	15.606 ± 0.018
	2526.8853	*R*	19.502 ± 0.038	15.439 ± 0.039
	2526.9912	*R*	19.595 ± 0.016	15.532 ± 0.017
	2526.9978	*I*	19.575 ± 0.035	...
	2527.0026	*B*	20.828 ± 0.026	...
	2527.0075	*V*	20.147 ± 0.022	...
	2527.0994	*R*	19.652 ± 0.018	15.589 ± 0.019
	2527.1041	*I*	19.364 ± 0.035	...
	2527.1089	*B*	20.591 ± 0.024	...
	2527.1136	*V*	19.885 ± 0.018	...
	2527.1184	*R*	19.498 ± 0.016	15.435 ± 0.017
2002 Nov 5	2527.1233	*R*	19.497 ± 0.016	15.434 ± 0.017
	2583.7588	*R*	20.210 ± 0.028	15.562 ± 0.029
	2583.7759	*R*	20.399 ± 0.033	15.751 ± 0.034
	2583.7937	*R*	20.212 ± 0.027	15.564 ± 0.028
	2583.8511	*R*	20.364 ± 0.033	15.716 ± 0.034
	2583.8977	*R*	19.950 ± 0.022	15.302 ± 0.023
2002 Nov 6	2583.9360	*R*	20.262 ± 0.028	15.614 ± 0.029
	2584.7529	*R*	20.103 ± 0.024	15.430 ± 0.025
	2584.7800	*R*	20.427 ± 0.033	15.754 ± 0.034
	2584.8093	*R*	20.168 ± 0.027	15.495 ± 0.028
	2584.8372	*R*	20.151 ± 0.026	15.478 ± 0.027
2002 Nov 7	2584.8845	*R*	20.110 ± 0.023	15.437 ± 0.024
	2585.7429	*R*	20.330 ± 0.027	15.634 ± 0.028
	2585.7476	*R*	20.222 ± 0.024	15.526 ± 0.025
	2585.7522	*R*	20.138 ± 0.022	15.442 ± 0.023
	2585.7920	*R*	20.467 ± 0.030	15.771 ± 0.031
	2635.7366	*R*	20.977 ± 0.061	15.388 ± 0.061
	2635.7419	*I*	20.521 ± 0.087	...
	2635.7467	*B*	21.988 ± 0.077	...
	2635.7515	*V*	21.501 ± 0.077	...
	2635.7563	*R*	21.087 ± 0.064	15.498 ± 0.064
	2635.7610	*I*	20.735 ± 0.104	...
	2635.7660	*B*	22.391 ± 0.117	...
	2635.7712	*V*	21.672 ± 0.095	...
	2635.7769	*R*	21.308 ± 0.084	15.719 ± 0.084

TABLE 3 —*Continued*

UT Date	JD (2,450,000+)	Filter	Observed Magnitude[a]	Absolute Magnitude[b]
2002 Dec 27	2635.7815	*R*	21.407 ± 0.096	15.818 ± 0.096
	2635.7864	*R*	21.345 ± 0.092	15.756 ± 0.092
	2635.7910	*R*	21.150 ± 0.076	15.561 ± 0.076
	2635.7959	*R*	20.969 ± 0.066	15.380 ± 0.066
	2635.8008	*R*	21.000 ± 0.069	15.411 ± 0.069
	2635.8054	*R*	20.985 ± 0.072	15.396 ± 0.072
	2635.8103	*R*	21.141 ± 0.086	15.552 ± 0.086
	2635.8149	*R*	21.079 ± 0.081	15.490 ± 0.081
	2635.8198	*R*	21.214 ± 0.089	15.625 ± 0.089
	2635.8250	*R*	21.218 ± 0.092	15.629 ± 0.092
2002 Dec 28	2635.8298	*R*	21.195 ± 0.094	15.606 ± 0.094
	2636.7263	*R*	21.443 ± 0.072	15.840 ± 0.072
	2636.7318	*I*	20.891 ± 0.117	...
	2636.7366	*B*	22.151 ± 0.086	...
	2636.7414	*V*	21.447 ± 0.070	...
	2636.7461	*R*	20.992 ± 0.045	15.389 ± 0.046
	2636.7512	*R*	21.017 ± 0.046	15.414 ± 0.047
	2636.7559	*R*	21.015 ± 0.046	15.412 ± 0.047
	2636.7803	*R*	21.090 ± 0.051	15.487 ± 0.051
	2636.7852	*R*	21.031 ± 0.048	15.428 ± 0.049
	2636.7903	*R*	21.483 ± 0.073	15.880 ± 0.073
	2636.7952	*R*	21.447 ± 0.073	15.844 ± 0.073

NOTE.—Obtained from observing runs in 2002 detailed in Table 2.
[a] Absolute photometric measurements of nucleus magnitude, uncorrected for distance or phase angle.
[b] Absolute magnitude of nucleus, normalized to $R = 1$ AU, $\Delta = 1$ AU, and $\alpha = 0°$.

Sheppard, & Fernández 2003), as well as C-type asteroids ($\beta_{\rm mean} \approx 0.043$ mag deg^{-1}; references in Belskaya & Shevchenko 2000). The large β suggests (but does not prove) that EP has a low-albedo, possibly porous surface.

Using an algorithm similar to that used to fit the linear phase function, we also estimated parameters for the IAU (H, G)-system (Bowell et al. 1989). We find best-fit parameters of $H_R = 15.3 \pm 0.1$ mag and $G_R = 0.026 \pm 0.1$. The quantity H_R corresponds to $m_R(1, 1, 0)$ in the linear phase function, and like the large value we calculate for β, the small G_R value is suggestive of a low-albedo surface. Fits for linear and IAU phase-magnitude relations are plotted in Figure 1.

From H_R, we estimate the effective radius, r_e, of the EP nucleus from

$$p_R r_e^2 = (2.24 \times 10^{22}) \times 10^{0.4[m_\odot - m_R(1,1,0)]}, \qquad (3)$$

where p_R is the geometric R-band albedo (Russell 1916), assumed to be $p_R = 0.04$, and $m_\odot = -27.07$ mag (Hardorp 1980; Hartmann et al. 1982, 1990) is used for the apparent solar R-band magnitude. Solving for the effective nucleus radius using our IAU result, H_R, for the absolute R-band magnitude gives $r_e = 2.5 \pm 0.1$ km. The quoted uncertainty is an estimate only but is expected to be dominated by the uncertain albedo of the nucleus. For example, if p_R is 2 times larger than we assume, then r_e would be $\sqrt{2}$ times smaller, or about $r_e = 1.8$ km.

This calculated radius is less than half the value of $r_e = 5.35$ km estimated by Tóth (2000) using the same assumed albedo of 0.04. This discrepancy is due to Tóth's use of a far brighter absolute magnitude, $m_V(1, 1, 0) = 14.0$, than we derived here. As our phase function fits are based on resolved light curves, in contrast to the isolated magnitude points (many of which are of highly questionable accuracy and

TABLE 4
2003 NUCLEUS PHOTOMETRY FOR 133P/ELST-PIZARRO

UT Date	JD (2,450,000+)	Filter	Observed Magnitude[a]	Absolute Magnitude[b]
2003 Sep 22.....	2905.1191	*R*	21.651 ± 0.066	15.698 ± 0.066
	2905.1216	*R*	21.681 ± 0.066	15.728 ± 0.066
	2905.1238	*R*	21.661 ± 0.066	15.708 ± 0.066
	2905.1260	*V*	22.026 ± 0.042	16.073 ± 0.043
	2905.1282	*B*	22.662 ± 0.197	16.709 ± 0.197
	2905.1304	*R*	21.721 ± 0.066	15.768 ± 0.066
	2905.1333	*V*	22.184 ± 0.047	16.231 ± 0.048
	2905.1360	*B*	22.475 ± 0.207	16.522 ± 0.207
	2905.1382	*R*	21.855 ± 0.076	15.902 ± 0.076

NOTE.—Obtained from 2003 Keck I observing run detailed in Table 2.
[a] Absolute photometric measurements of nucleus magnitude, uncorrected for distance or phase angle.
[b] Absolute magnitude of nucleus, normalized to $R = 1$ AU, $\Delta = 1$ AU, and $\alpha = 0°$.

TABLE 5
133P/Elst-Pizarro Colors

UT Date	JD (2,450,000+)	$B-V$	$V-R$	$R-I$
2002 Sep 9.....	2527.00	0.68 ± 0.04	0.49 ± 0.05	0.17 ± 0.05
2002 Dec 27	2527.10	0.71 ± 0.03	0.36 ± 0.05	0.24 ± 0.05
	2635.74	0.49 ± 0.11	0.35 ± 0.10	0.47 ± 0.11
	2635.76	0.72 ± 0.15	0.36 ± 0.13	0.54 ± 0.12
2002 Dec 28	2636.73	0.70 ± 0.11	0.41 ± 0.08	0.23 ± 0.14
2003 Sep 22.....	2905.13	0.64 ± 0.20	0.35 ± 0.08	...
	2905.14	0.29 ± 0.21	0.41 ± 0.08	...
Mean[a]	...	0.69 ± 0.02	0.41 ± 0.03	0.27 ± 0.03

[a] Weighted means (averaged in flux space) of colors, reported in magnitudes. Errors listed are uncertainties on calculated means.

precision) available to Tóth, we believe that our absolute magnitude and resulting size estimate are reliable.

We searched for periodicity in the absolute R-band magnitudes of the nucleus using the phase dispersion minimization (PDM) algorithm described by Stellingwerf (1978) and coded by M. Buie. This method minimizes scatter in a given data set phased to a series of test periods and makes no assumption about the shape of the light curve. This is useful given that the irregular nucleus shapes of comets and asteroids may produce highly nonsinusoidal light curves. One disadvantage is that the technique does not discern multiple periodicities that might be present in the light curve of an irregularly shaped body with significant non–principal-axis rotation.

A period-likelihood plot generated from our 2002 data set is shown in Figure 2, where the likelihood of a given test period is given by the parameter Θ. The minimum value for Θ, indicated by the deepest downward spike on the period-likelihood plot, represents the minimum dispersion of data points for a given rotational period and, therefore, the most likely solution. The deepest spike on the plot shown corresponds to $P_{\rm rot} = 3.471 \pm 0.001$ hr as the best rotational period solution for EP, though a secondary spike indicates another possible period of $P_{\rm rot} = 1.736 \pm 0.001$ hr, exactly half that of the primary period. Uncertainties are estimated from the range of different periods given by the PDM routine for slightly different initial fit parameters.

When we phase our phase-angle–normalized, reduced-magnitude data to a $P_{\rm rot} = 3.471$ hr rotational period, several magnitude points are found to be quite divergent from the main light curve. Closer inspection reveals that many of these points were obtained on our December observing run, during which the comet was at its faintest (being at its largest geocentric distance and largest phase angle). During this run, the seeing was also relatively poor and variable (ranging from 1.″0 to 1.″5), leading to large photometric uncertainties.

With this in mind, we removed magnitude measurements in the original data set for which uncertainties exceed 0.05 mag and repeated the PDM and data-phasing analysis. Removing these points does not appreciably change the appearance of the period-likelihood plot in Figure 2 or the numerical value of the most likely rotational period output by the PDM routine (which accounts for uncertainties of input data), but it substantially improves the appearance of the double-peaked light curve shown in Figure 3. Phasing the data to the second rotational period found above ($P_{\rm rot} = 1.736$ hr) results in a single-peaked light curve that, as expected given the asymmetric appearance of the double-peaked light curve, is not as cleanly defined as the double-peaked curve.

TABLE 6
Rotationally Averaged 133P/Elst-Pizarro Photometry

UT Date	α (deg)	Mean Magnitude	Reduced Magnitude
2002 Aug 19.....	14.50	20.10 ± 0.10	16.26 ± 0.10
2002 Sep 7–9	8.15	19.70 ± 0.05	15.97 ± 0.05
2002 Nov 5–7	13.57	20.25 ± 0.05	16.17 ± 0.05
2002 Dec 27–28.....	18.73	21.20 ± 0.05	16.43 ± 0.05

Note.—Rotationally averaged magnitude values for 133P/Elst-Pizarro from estimated midpoints of light curves plotted for four separate observing runs in 2002. Observing run details are listed in Table 2. Data are used to determine magnitude dependence on phase angle, α, as plotted in Fig. 1.

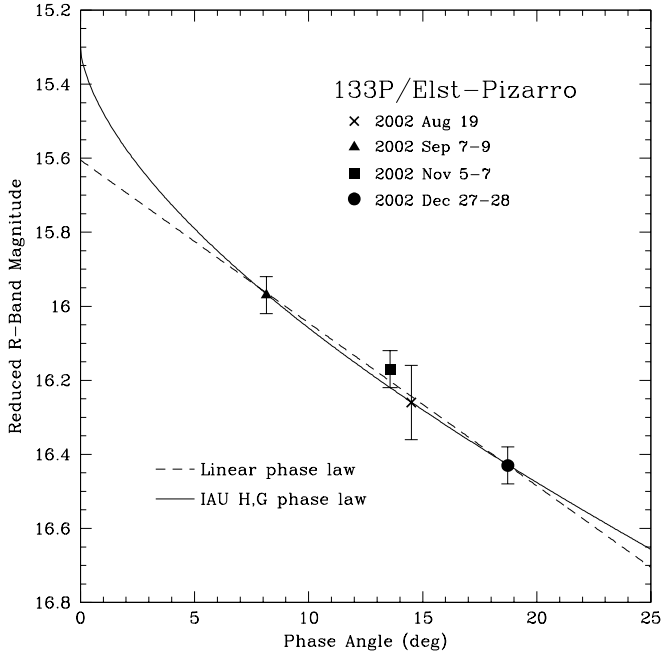

Fig. 1.—Phase functions for 133P/Elst-Pizarro. Points are rotationally averaged nucleus magnitudes (normalized to heliocentric and geocentric distances of 1 AU; tabulated in Table 6) from four observing runs in 2002 detailed in Table 2. The dashed line represents a linear least-squares fit, specified by eq. (2), where $m_R(1, 1, 0) = 15.61 \pm 0.01$ mag and $\beta = 0.044 \pm 0.007$ mag deg^{-1}. The solid line represents an IAU (H, G) model fit ($H_R = 15.3 \pm 0.1$ mag and $G_R = 0.026 \pm 0.1$), which includes an assumed opposition surge at small phase angle.

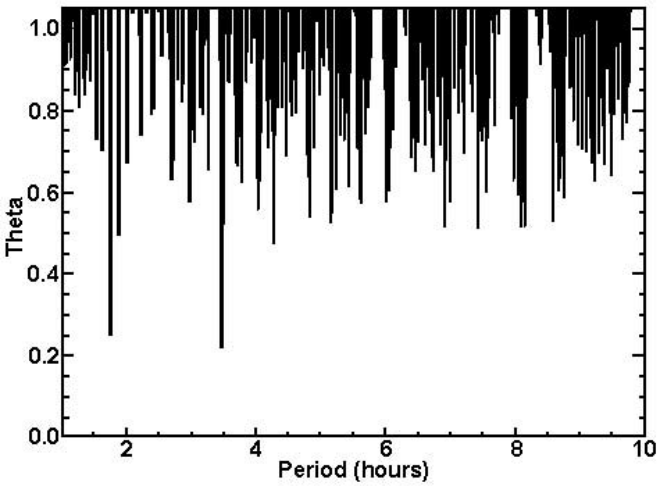

FIG. 2.—Period-likelihood plot produced by phase dispersion analysis of phase-angle–normalized, reduced-magnitude data for 133P/Elst-Pizarro. The deepest downward spike indicates the most likely period fit, corresponding here to a double-peaked rotational period of $P_{\rm rot} = 3.471$ hr.

The two-peaked nature of the best rotational light curve we find for EP suggests that we are observing modulation of the scattering cross section of the body due to an aspherical shape. A light curve caused by surface albedo variation would be single-peaked, and furthermore, observations of other asteroids and comets show that albedo modulation as large as in Figure 3 is exceedingly rare. The peak-to-peak photometric range, $\Delta m_R = 0.40 \pm 0.05$ mag, implies that the ratio of the axes of the body projected onto the plane of the sky is approximately

$$a/b = 10^{0.4\Delta m_R} = 1.45 \pm 0.07. \quad (4)$$

Equation (4) gives a lower limit to the true ratio of the axes because of projection effects. Taking EP's cross-sectional shape to be approximately that of an ellipse, where $r_e^2 = a \times b$, we find $a \sim 3.0$ km and $b \sim 2.1$ km as our best estimates of the semiaxes of the nucleus.

We conclude that EP is a modestly sized, elongated object in rapid rotation. With a 3.471 hr rotational period, EP is the fastest rotator among comets for which rotational periods are known (see, e.g., tables in Jewitt 1996 and Jorda & Gutiérrez 2002), followed by P/Schwassmann-Wachmann 2 at $P_{\rm rot} = 5.58 \pm 0.03$ hr (Luu & Jewitt 1992a). EP's rotational period is less unusual among small asteroids. For example, in a study of 26 near-Earth objects (NEOs) with absolute magnitudes $H_V = 13.6$–20.0 (effective radii approximately 0.2–4 km), Pravec, Wolf, & Šarounová (1998) found eight with $P_{\rm rot} < 3.7$ hr. Notably, 1943 Anteros, which with $H_R = 15.41 \pm 0.13$ is a reasonable size analog to EP ($H_R = 15.3 \pm 0.1$), was found to have $P_{\rm rot} = 2.8695 \pm 0.0002$ hr.

If photometric variation is caused by object elongation and not by albedo gradients, this suggests that the majority of these objects are effectively strengthless rubble piles, and so those with larger elongations simply cannot survive at higher rotation rates without breaking apart. Earlier, we found a photometric peak-to-peak range of $\Delta m_R = 0.40 \pm 0.05$ mag for EP. Thus, while EP's spin rate is unusual among comets whose rotational periods are known, it is typical for other asteroidal NEOs of comparable elongation. What this implies about the proper physical classification of EP, as a comet or asteroid, is unclear, however.

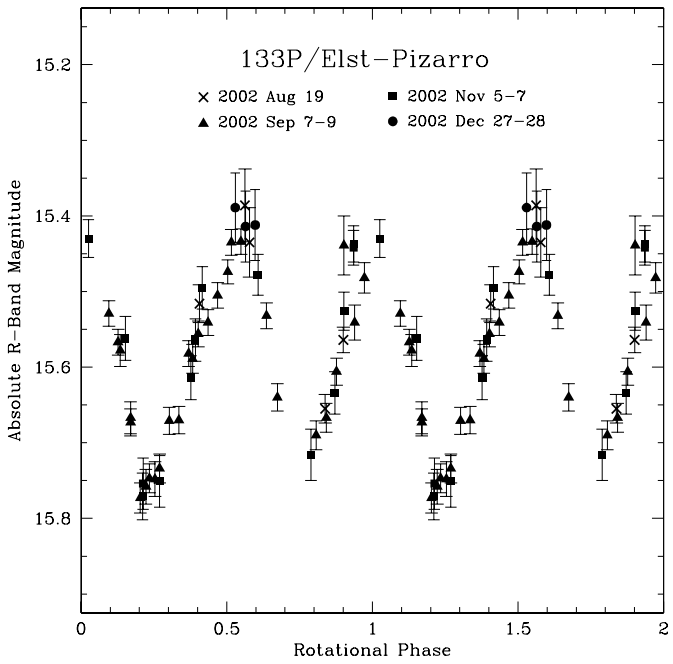

FIG. 3.—Phase-angle–normalized, reduced-magnitude data for observations of 133P/Elst-Pizarro made between 2002 August and December, phased to a rotational period of $P_{\rm rot} = 3.471$ hr, where magnitude measurements with uncertainties exceeding 0.05 mag (mostly from our December run, when seeing was poor) have been removed.

3.2. *Centripetal Limit*

The critical density that a prolate body rotating with a period $P_{\rm rot}$ about its short axis, b, must possess for self-gravity to balance centripetal acceleration can be estimated from

$$\rho_{\rm crit} \approx 1000\left(\frac{3.3^h}{P_{\rm rot}}\right)^2\left(\frac{a}{b}\right), \quad (5)$$

where $\rho_{\rm crit}$ is the critical bulk density of the nucleus in kilograms per cubic meter and a/b is the long-to-short axis ratio of the nucleus (Harris 1996). By inserting the values for $P_{\rm rot}$ and a/b that we determine for EP, we can obtain the minimum density needed to ensure that the EP nucleus is not in a state of internal tensile stress. We find $\rho_{\rm crit} = 1300$ kg m^{-3} by this method.

Observations of other asteroids show that only the tiniest, those with diameters $\lesssim 0.1$ km, possess internal tensile strength large enough to spin faster than the centripetal limit (Pravec et al. 2000; Whiteley, Tholen, & Hergenrother 2002). These small objects are likely structural monoliths, liberated by impact from larger parent bodies, and are too small to constitute good analogs for EP. All larger asteroids rotate more slowly than the centripetal limit and hence appear to lack tensile strength. We suggest that EP is most likely a structurally weak body, with a bulk nucleus density near $\rho_n = 1300$ kg m^{-3} and rotating near or at the centripetal limit.

4. THE DUST TRAIL

In our initial 2002 August 19 trail rediscovery images, EP's dust trail was visible even in a single 300 s exposure. We combined multiple images, aligned on the photocenter of the nucleus, to produce a single composite image with higher signal-to-noise ratio than any of the individual images. We obtained our brightest image of the trail in 2002 September

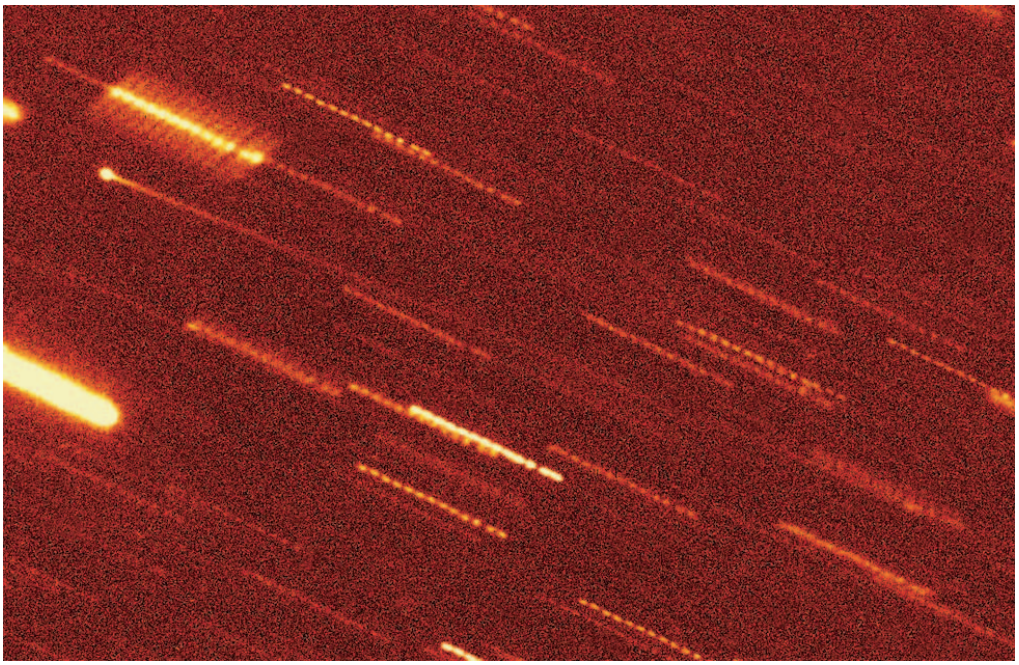

FIG. 4.—Composite *R*-band image of 133P/Elst-Pizarro from UT 2002 September 7 observations on the University of Hawaii 2.2 m telescope. The nucleus is at upper left with the dust trail extending across the entire field, down and to the right. The image is 2′.5 by 3′.5 in size, with north at the top and east to the left.

(Fig. 4) and note that the trail faded slightly in November and nearly disappeared by December (Fig. 5).

In follow-up images taken with Keck I almost a year later on 2003 September 22, the trail was completely absent. The 500 s composite image (Fig. 6) we obtained with Keck is equivalent in depth to a 10,000 s exposure at the smaller UH 2.2 m telescope. A trail as bright as any shown in Figure 5 would be easily visible in this image. As no trail was observed in images obtained from Keck, all following discussion regarding the EP dust trail refers to 2002 observations.

The surface brightness profile and width of our observed trails provide constraints on the nature of the dust emitted by EP. Time dependence of the trail, discussed later, is a third constraint.

4.1. *Trail Surface Brightness*

To measure surface brightnesses of the trails, we first rotate each composite image to make the trail horizontal in the image frame. We then determine surface brightness using rectangular apertures, measuring 20 by 10 pixels (4″.38 by 2″.19, chosen to be much wider than the nightly seeing so as to capture all light from the trail even under substandard seeing conditions), with sky background determined from two square 10 by 10 pixel (2″.19 by 2″.19) apertures placed above and below the segment of the trail being measured. An illustration of the scheme is shown in Figure 7. In cases where a sky background sample appears contaminated by background stars or galaxies, its counterpart sky sample on the opposite side of the trail or an interpolation between immediately adjacent sky samples is used as a substitute.

This procedure is extended from the nucleus itself (measured inside a 20 by 20 pixel box, approximately the size of the aperture used for our original nucleus photometry, with 20 by 10 pixel sky samples as shown in Fig. 7) along the length of the trail. The trail surface brightness, in counts per linear arcsecond along the length of the trail, is normalized to the average count rate measured for the comet nucleus. We do this to minimize inverse square brightness variations caused by EP's varying heliocentric and geocentric distances. Uncertainties shown are derived from rms variations in individual pixel values measured within nearby sky background segments.

This procedure is performed for images in all available filters: *B*, *V*, *R*, and *I*. Unfortunately, we have only 600 s of effective exposure time available in each of the *B*, *V*, and *I* filters in September and a largely faded trail in December. The low signal-to-noise ratio, even close to the nucleus, in composite images for these other filter bands prevents us from achieving any meaningful color measurements of the trail. Thus, for the remainder of our analysis we consider only *R*-band data.

Surface brightness profiles are shown in Figure 8, with numerical data listed in Table 7. While we can visually trace the trail for almost 3′.5 ($\sim 4.5 \times 10^8$ m in the plane of the sky) in September, useful surface brightness measurements are possible only to about 1′.5 (about 2×10^8 m). The basic parameters of the trail within this distance include declining surface brightness along the trail, varying with distance from the nucleus, γ, approximately as $\gamma^{-0.6}$, and a characteristic width perpendicular to the trail slightly larger than the FWHM seeing.

We also compute mean surface brightness values, again normalized to the brightness of the EP nucleus, averaged over larger rectangular bins along the length of the trail. The process starts as before, except with unit apertures only 1 pixel long (0″.219 long, along the length of the trail). Apertures are still all 20 pixels wide (4″.36) in the direction perpendicular to the trail, and uncertainties are again derived from rms variations in pixel values measured within nearby sky background segments. Surface brightness values from individual apertures are then combined into bins and averaged. Lengths of the bins along the trail vary from 5 pixels (1″.09) near the nucleus, where the surface brightness gradient is very steep, to 20 pixels (4″.36) along the more distant, fainter segments of the trail. We tabulate these mean brightnesses in Table 8, in which the first

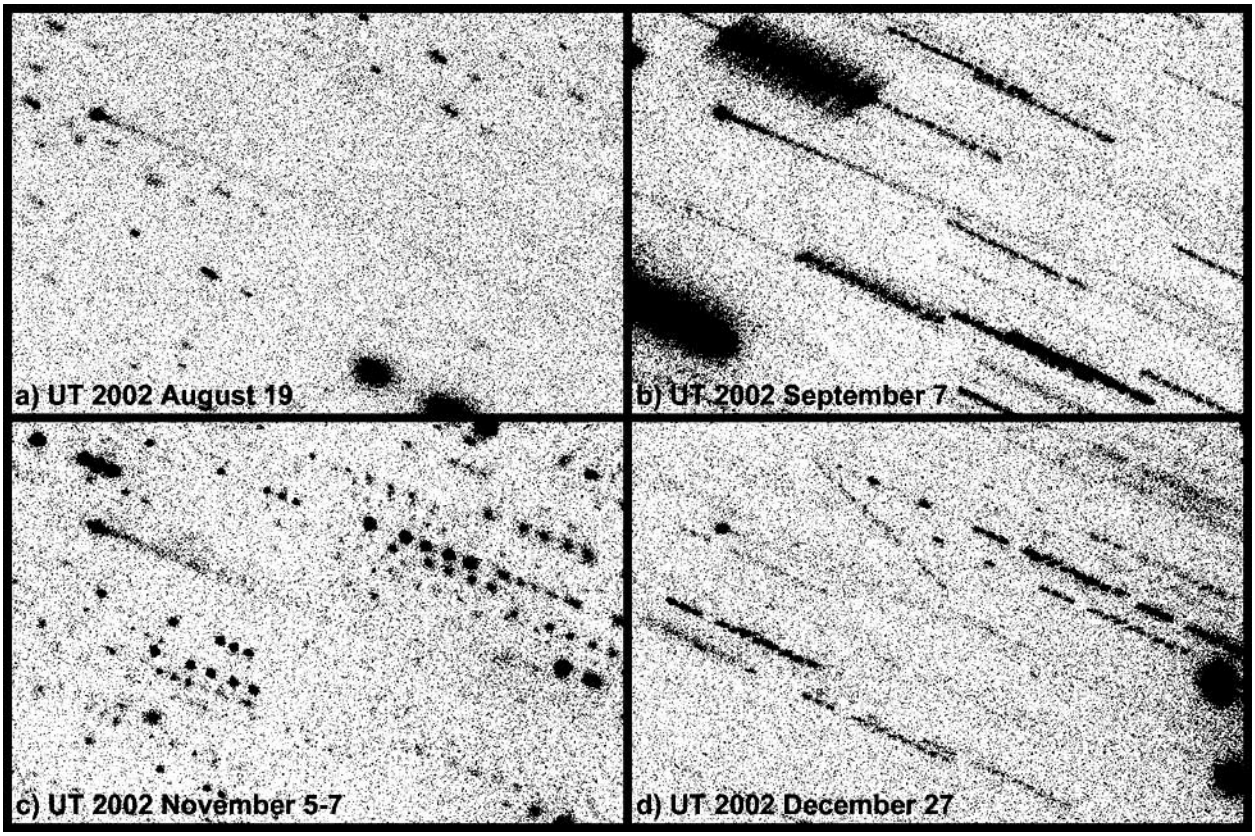

FIG. 5.—Small composite *R*-band images of 133P/Elst-Pizarro from observations on the University of Hawaii 2.2 m telescope on UT 2002 (*a*) August 19, (*b*) September 7, (*c*) November 5–7, and (*d*) December 27. Images represent 2500, 3900, 4500, and 4200 s in effective exposure time, respectively. Each image is approximately 2′ by 1.′5 in size, with north at the top and east to the left. Observing conditions are listed in Table 2. The nucleus is held at the same position in each image in the upper left corner, with the dust trail extending down and to the right. Shorter, dotted trails and/or pointlike sources are background stars, galaxies, or crossing field asteroids.

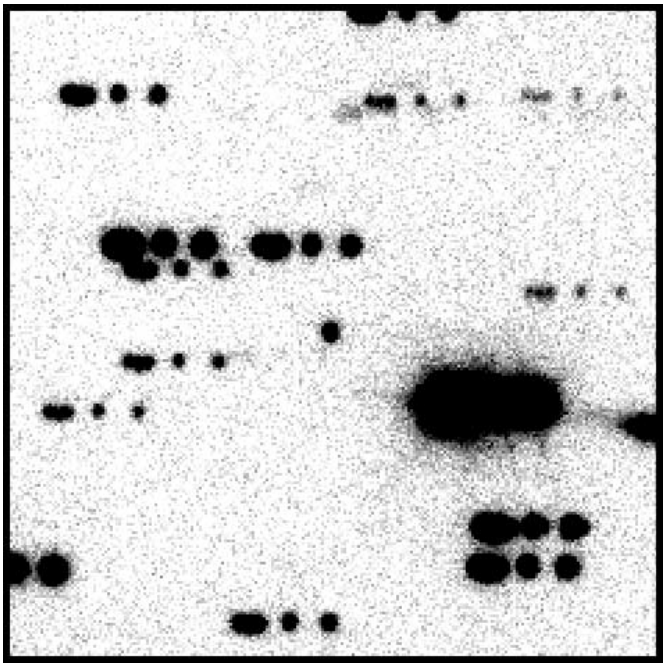

FIG. 6.—Composite *R*-band image of 133P/Elst-Pizarro (center of frame) from UT 2003 September 22 observations on the 10 m Keck I Telescope. The image represents 500 s in effective exposure time, equivalent to 10,000 s of exposure time on the smaller UH 2.2 m telescope. The field of view is 1 arcmin^2, with north at the top and east to the left.

three columns list the positions of the inner and outer edges of the averaging boxes, and of the box centers, respectively. The mean surface brightness of trails imaged during each observing run are listed in the next four columns, together with the error on the mean within each box. The table clearly shows that surface brightness faded only slightly in the interval between August and November but faded by a factor of about 3 in December. This strong fading is emphasized in Figure 9, where surface brightness profiles from August and December are plotted together.

While normalizing trail brightness to nucleus brightness compensates for inverse square falloff in both solar illumination of EP and reflected light received on Earth, there are other geometric effects to consider. Assuming the trail is an optically thin sheet of material oriented perpendicularly to the plane of the sky, the projected column density varies with phase angle α. The exact variation depends on factors such as orientation, shape, and inherent surface density distribution of the sheet. We note though that the trail brightness changed relatively little between August and November, during which period α varied by over 6°, whereas α changed by only 4° during the trail's sudden fading in December. Thus, change in phase angle is unlikely to be a primary cause of trail fading.

Another effect is the variation of particle column density due to the change in physical length of trail subtended by a given angle seen projected on the sky. With EP at a distance of $\Delta = 2.05$ AU from Earth in August, each linear arcsecond subtended about 1500 km along the trail. In December

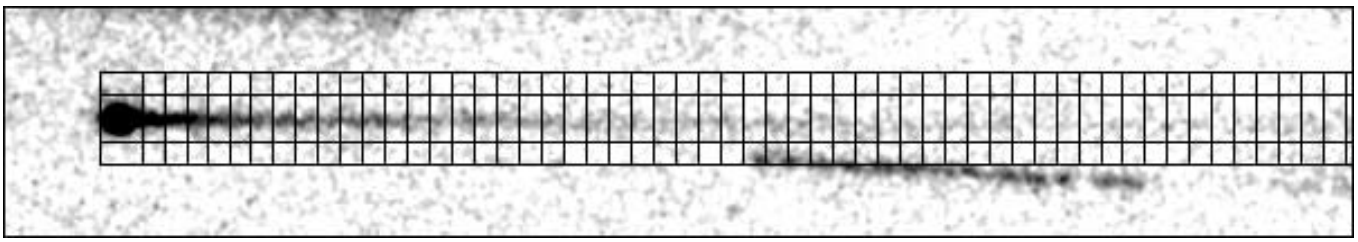

FIG. 7.—Schematic diagram for measurement of trail surface brightness. This composite *R*-band image comprises 13, 300 s exposures on 2002 September 7, is rotated to make the trail horizontal in image frame, and measures 0.′4 by 2.′2. Individual rectangular apertures placed on the trail are approximately 2″ by 4″, while square apertures used to measure sky background are 2″ by 2″. The nonhorizontal dotted streak is a trailed field star.

$\Delta = 2.93$ AU, and so each linear arcsecond then subtended 2100 km. This increase in subtended trail distance implies that for a temporally invariant trail, column density and thus apparent surface brightness should actually increase in December, which is opposite to what was observed.

Finally, the change in EP's orbit-plane angle, $\alpha_{\rm pl}$, must be considered, since an appreciable tilting of the optically thin sheet of ejected material that we observe as EP's trail could reduce its observed surface brightness, making it more difficult to detect over sky background. For an infinitely thin sheet of trail material, projected thickness, $w_{\rm proj}$, can be approximated by $w_{\rm proj} \sim w_1|\sin \alpha_{\rm pl}|$, where w_1 is a constant representing a characteristic width of the surface of the sheet. Assuming a more realistic three-dimensional slab of trail material with finite thickness, w_2, the projected thickness then roughly becomes $w_{\rm proj} \sim w_1|\sin \alpha_{\rm pl}| + w_2 \cos \alpha_{\rm pl}$, where it should be noted that $w_1 \gg w_2$. We recall however that surface brightness measurements were made with apertures much larger than the observed trail widths to allow for variable seeing conditions, but they could allow for substantial changes in projected trail width as well. We also recall that trail fading is slight between September and November, during which period $\alpha_{\rm pl}$ changes the most (from 0.°1 to 0.°6), while the dramatic fading in December occurs at an $\alpha_{\rm pl}$ that is actually intermediate (0.°4) between those values. We therefore find that the trail fading observed in December cannot be caused by changes in the projected trail thickness. Thus, having ruled out all possible geometric causes for observed changes in trail brightness, we conclude that the fading we observed was intrinsic to the trail.

One caveat in our analysis is that we assume that dust grains were nonvolatile and disappeared only upon dispersal at large distances from the nucleus, becoming too diffuse to be detectable. If the dust trail were partially composed of volatile material, such as water ice grains that sublimated soon after being released from the nucleus, then the dust trail's behavior would become much more difficult to simulate. Hanner (1981) found, however, that only grains of very pure water ice could survive for very long at $R \sim 2.5$ AU. The presence of even trace amounts of absorbent material reduced grain lifetimes to a matter of hours or less. We observed EP's dust trail to persist for much longer, of course, and furthermore, such a short lifetime would restrict the maximum dispersion of grains from the nucleus to a few hundred kilometers, not the hundreds of thousands of kilometers that the dust trail was observed to span. Thus, in this analysis, we assume that the contribution of sublimating icy grains to the EP dust trail is negligible.

By integrating surface brightness profiles, we can estimate the mass-loss rate and, therefore, EP's level of activity. Integrating over the first 90″ of the trail in August, September, November, and December, and roughly interpolating across trail segments contaminated by crossing field asteroids, we find that the ratios of the total flux in the dust trail to that from the EP nucleus were $F_{d,\rm Aug} \sim 1.3$, $F_{d,\rm Sep} \sim 1.3$, $F_{d,\rm Nov} \sim 1.1$, and $F_{d,\rm Dec} \sim 0.6$. The effective cross-sectional area of the EP nucleus is $C_n = \pi r_e^2 \sim 20$ km^2. Assuming the dust and nucleus to have the same albedo, we estimate the total cross section in dust as $C_{d,\rm Aug} = F_d C_n \sim 26$ km^2, $C_{d,\rm Sep} \sim 26$ km^2, $C_{d,\rm Nov} \sim 22$ km^2, and $C_{d,\rm Dec} \sim 12$ km^2. If the average particle radius in the trail is a_d, the number of particles is $N_d = C_d/(\pi a_d^2)$ and their total mass is $M_d \sim (4/3)\pi \rho_d a_d^3 N_d$, or

$$M_d \sim (4/3)\rho_d a_d C_d. \tag{6}$$

Assuming $\rho_d \sim 10^3$ kg m^{-3} and $a_d \sim 5$ μm (see below), we obtain $M_{d,\rm Aug} \sim 1.7 \times 10^5$ kg, $M_{d,\rm Sep} \sim 1.7 \times 10^5$ kg, $M_{d,\rm Nov} \sim 1.5 \times 10^5$ kg, and $M_{d,\rm Dec} \sim 0.8 \times 10^5$ kg. From August to September, the overall trail brightness stayed roughly constant (though it declined close to the nucleus) and then faded to its November level in 60 days and finally to its December level about 50 more days later. We therefore find approximate net mass-loss rates from the trail of $\lesssim 0.001$ kg s^{-1} between August and September, ~ 0.005 kg s^{-1} between September and November, and ~ 0.016 kg s^{-1} between November and December, which are probably accurate, at best, to order of magnitude.

These trail mass-loss rates represent a combination of absolute mass loss from the trail (due to dissipation) and mass injection from the nucleus into the trail. The fading of the trail between August and December indicates that the dust injection rate became smaller than the absolute dissipation rate, leading to a net disappearance of the trail. Assuming the physical makeup of the trail (in terms of grain sizes and dust composition) did not change appreciably over the observing period, the absolute mass-loss rate from the trail should have remained approximately constant. The increasing net trail dissipation rate then implies that the dust injection rate was slowing.

Intuitively, this paints a picture of EP in which dust was being actively released by the nucleus into the trail for many months before slowing and eventually stopping, leading to the disappearance of the trail. A similar picture was also developed for the EP trail in 1996. These interpretations taken together strongly imply that both emission events were cometary in nature (i.e., driven by sublimation of volatile material), and not the result of impacts as Tóth (2000) suggested for the 1996 trail apparition. We will investigate this possibility further later in this paper.

4.2. *Trail Width*

The trail width in our 2002 September images (in which we obtained the best signal-to-noise ratio for the trail) is shown as

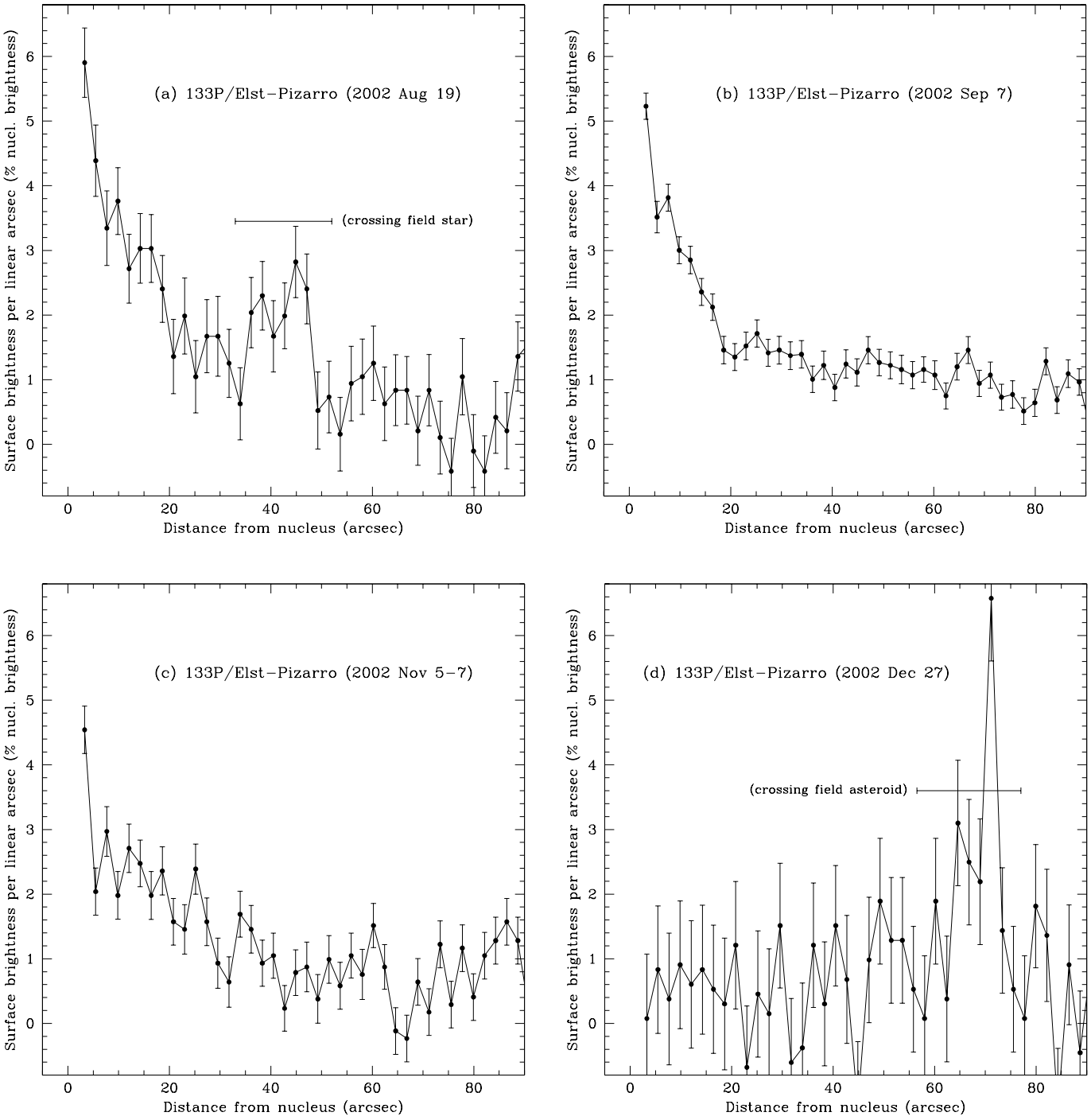

FIG. 8.—Surface brighness profiles of the 133P/Elst-Pizarro dust trail, normalized to nucleus brightness, for composite images from observations made on 2002 August 19 (2500 s effective exposure time), September 7 (3900 s), November 5–7 (4500 s), and December 27 (4200 s). For average *R*-band nucleus magnitudes of 20.1 in August, 19.7 in September, 20.2 in November, and 21.1 in December, one surface brightness unit is equivalent to 25.1, 24.7, 25.2, and 26.1 mag per linear arcsecond, respectively.

TABLE 7

133P/Elst-Pizarro Dust Trail Photometry: 2002

	2002 Aug 19		2002 Sep 7		2002 Nov 5–7		2002 Dec 27	
Position[a]	% Nuc.	Error	% Nuc.	Error	% Nuc.	Error	% Nuc.	Error
3.3	5.90	0.54	5.23	0.20	4.54	0.37	0.08	1.00
5.5	4.39	0.55	3.52	0.24	2.04	0.36	0.83	0.99
7.7	3.34	0.58	3.82	0.21	2.97	0.38	0.38	1.02
9.9	3.76	0.52	3.00	0.21	1.98	0.37	0.91	0.99
12.0	2.72	0.53	2.85	0.21	2.71	0.38	0.60	0.99
14.2	3.03	0.54	2.36	0.21	2.48	0.36	0.83	1.00
16.4	3.03	0.52	2.12	0.20	1.98	0.37	0.53	0.99
18.6	2.40	0.52	1.46	0.21	2.36	0.37	0.30	1.02
20.8	1.36	0.58	1.35	0.21	1.57	0.36	1.21	0.99
23.0	1.99	0.59	1.52	0.21	1.46	0.38	−0.68	0.95
25.2	1.04	0.56	1.72	0.22	2.39	0.39	0.45	0.98
27.4	1.67	0.57	1.41	0.21	1.57	0.37	0.15	1.00
29.6	1.67	0.62	1.46	0.21	0.93	0.39	1.51	0.97
31.8	1.25	0.53	1.37	0.22	0.64	0.39	−0.60	0.99
33.9	0.63	0.56	1.39	0.21	1.69	0.36	−0.38	1.00
36.1	2.04	0.54	1.01	0.21	1.46	0.37	1.21	0.96
38.3	2.30	0.53	1.22	0.22	0.93	0.36	0.30	0.96
40.5	1.67	0.55	0.88	0.21	1.05	0.35	1.51	0.93
42.7	1.99	0.51	1.24	0.22	0.23	0.35	0.68	0.99
44.9	2.82	0.55	1.11	0.21	0.79	0.35	−1.29	1.00
47.1	2.40	0.54	1.46	0.21	0.87	0.38	0.98	0.97
49.3	0.52	0.60	1.26	0.20	0.38	0.38	1.89	0.97
51.5	0.73	0.55	1.22	0.21	0.99	0.37	1.29	0.97
53.7	0.16	0.57	1.16	0.22	0.58	0.36	1.29	0.97
55.8	0.94	0.58	1.07	0.21	1.05	0.35	0.53	0.97
58.0	1.04	0.58	1.16	0.20	0.76	0.39	0.08	0.97
60.2	1.25	0.58	1.07	0.22	1.51	0.34	1.89	0.97
62.4	0.63	0.57	0.75	0.20	0.87	0.35	0.38	0.97
64.6	0.84	0.55	1.20	0.21	−0.12	0.36	3.10	0.97
66.8	0.84	0.52	1.46	0.21	−0.23	0.36	2.49	0.97
69.0	0.21	0.53	0.94	0.20	0.64	0.36	2.19	0.97
71.2	0.84	0.55	1.07	0.20	0.17	0.36	6.58	0.97
73.4	0.10	0.56	0.73	0.20	1.22	0.36	1.44	0.97
75.6	−0.42	0.51	0.77	0.21	0.29	0.36	0.53	0.97
77.7	1.04	0.59	0.51	0.21	1.16	0.36	0.08	0.97
79.9	−0.10	0.56	0.64	0.21	0.41	0.36	1.81	0.95
82.1	−0.42	0.55	1.29	0.21	1.05	0.36	1.36	1.02
84.3	0.42	0.56	0.69	0.21	1.28	0.36	−1.36	0.97
86.5	0.21	0.59	1.09	0.21	1.57	0.36	0.91	0.93
88.7	1.36	0.54	0.96	0.21	1.28	0.36	−0.45	0.96
90.9	1.57	0.55	0.21	0.21	0.17	0.36	0.98	0.98

Note.—Listed are surface brightness measurements for composite images of 133P/Elst-Pizarro dust trails, expressed as percentages of nuclear brightness per linear arcsecond.

[a] Distance (projected on the sky) from comet nucleus in arcseconds.

TABLE 8

Trail Surface Brightness versus Time

x_{min}[a]	x_{max}[b]	x_{mean}[c]	2002 Aug 19[d]	2002 Sep 7[d]	2002 Nov 5–7[d]	2002 Dec 27[d]
2.30	3.18	2.74	6.96 ± 0.45	5.92 ± 0.55	5.30 ± 0.63	1.84 ± 0.90
3.39	4.27	3.83	4.85 ± 0.22	4.49 ± 0.26	3.85 ± 0.51	-1.26 ± 0.76
4.49	6.46	5.48	4.34 ± 0.48	3.49 ± 0.16	2.06 ± 0.35	0.96 ± 0.92
6.68	8.65	7.67	3.37 ± 0.56	3.82 ± 0.10	3.02 ± 0.14	0.48 ± 0.87
8.87	10.84	9.86	3.72 ± 0.57	2.99 ± 0.19	2.09 ± 0.29	1.15 ± 0.99
11.06	13.03	12.05	2.67 ± 0.58	2.83 ± 0.24	2.72 ± 0.29	0.63 ± 0.85
13.03	17.19	15.11	3.04 ± 0.33	2.24 ± 0.12	2.29 ± 0.20	0.58 ± 0.53
17.41	21.57	19.49	1.82 ± 0.35	1.45 ± 0.11	1.99 ± 0.19	0.82 ± 0.49

[a] Distance of inner edge of averaging box from nucleus, in arcseconds.

[b] Distance of outer edge of averaging box from nucleus, in arcseconds.

[c] Distance of middle of averaging box from nucleus, in arcseconds.

[d] Mean normalized surface brightness from data obtained on given UT date.

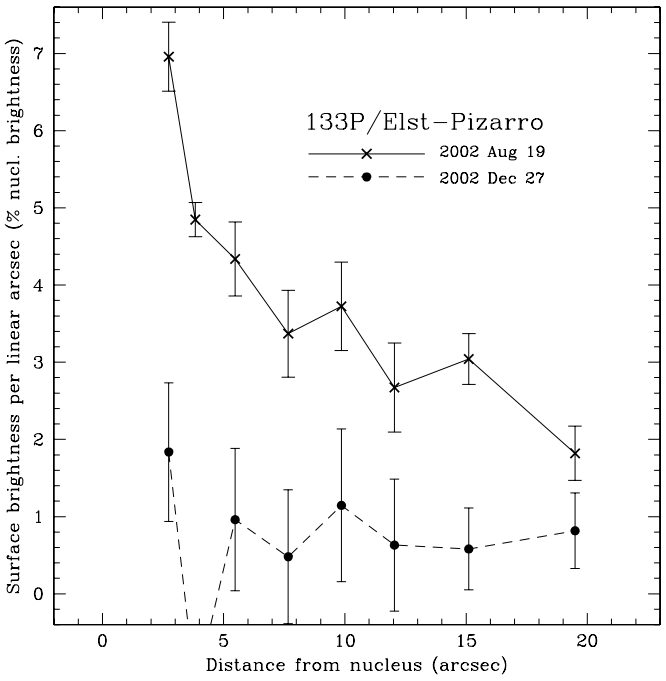

FIG. 9.—Comparison of the first 30″ of dust-trail profiles from 2002 August and December runs from data tabulated in Table 8. September and November data are omitted for clarity, to emphasize fading over entire observing period. For average *R*-band nucleus magnitudes of 20.1 in August and 21.1 in December, one surface brightness unit is equivalent to 25.1 and 26.1 mag per linear arcsecond, respectively.

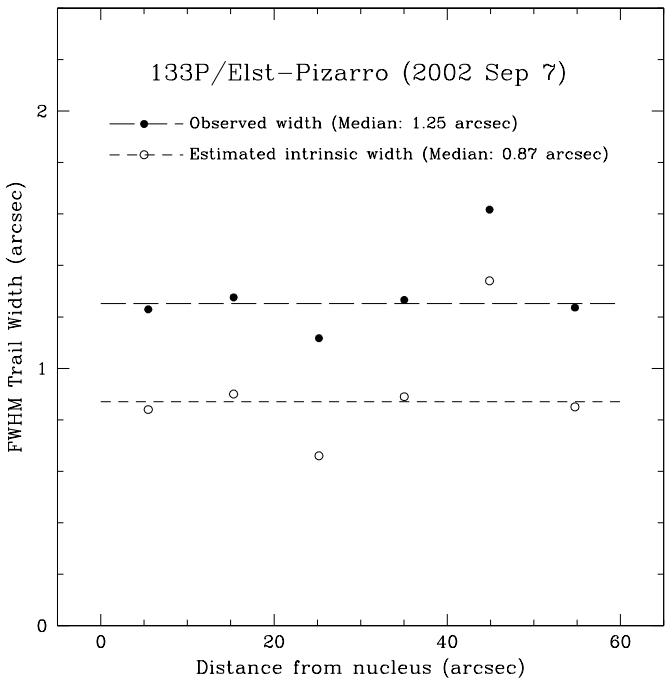

FIG. 10.—Observed and estimated intrinsic cross-sectional width (FWHM) in arcseconds of 133P/Elst-Pizarro's dust trail as a function of projected angular distance from the nucleus. Observed width is measured from the composite *R*-band image (3900 s) from 2002 September 7 and represents a convolution of intrinsic width and the atmospheric seeing. Intrinsic trail width is thus estimated from observed width and FWHM seeing measured from field stars in individual long-exposure images of other objects taken the same night (since field stars in EP images are trailed), as well as the EP nucleus in the composite image.

a function of γ in Figure 10. We plot both the observed FWHM of the trail, $\theta_o(\gamma)$, and an estimate of the intrinsic width, $\theta_i(\gamma)$, that would be observed in the absence of atmospheric seeing, θ_s. The latter is computed from

$$\theta_i(\gamma) = [\theta_o^2(\gamma) - \theta_s^2]^{1/2}, \tag{7}$$

where $\theta_s \sim 0\farcs8$ (FWHM) on September 7 for individual image frames but $\theta_s \sim 0\farcs9$ for the composite image. The figure shows that close to the nucleus, the intrinsic trail width was roughly $0\farcs9$ (FWHM), corresponding to about 1200 km, in the plane of the sky. We expect the trail to flare somewhat toward larger γ as dust particles drift away from the orbit plane, but we were unable to test for this effect because of low trail surface brightness far from the nucleus.

The trail's narrowness suggests that the optically dominant particles were launched from the nucleus at low relative velocity, since rapid ejection would produce a broad and divergent dust tail like those seen in many classical comets. Low ejection velocities suggest that the particles are large.

The absence of a resolved, spheroidal coma about the nucleus of EP independently suggests that the optically dominant grains are ejected slowly. Grains ejected sunward at relative speed v_g are turned around by solar radiation pressure on the distance scale

$$X_R \sim \frac{v_g^2 R^2}{2\beta_d g_\odot}, \tag{8}$$

where R is the heliocentric distance in AU and $g_\odot = 0.006$ m s^{-2} is the gravitational acceleration to the Sun at 1 AU (Jewitt & Meech 1987). The quantity β_d is the dimensionless ratio of the radiation pressure acceleration to the local gravity. Formally, β_d is a complicated function of the grain size, composition, and shape (Burns, Lamy, & Soter 1979), but it can also be approximated by

$$\beta_d \approx \frac{3\ L_\odot}{16\pi G M_\odot c}\frac{Q_{\rm pr}}{\rho_d a_d}, \tag{9}$$

where $L_\odot$ and $M_\odot$ are the solar luminosity and mass, G is the gravitational constant, c is the speed of light, and $Q_{\rm pr}$ is a radiation pressure efficiency factor. Later, we assume as a reasonable further approximation that $\beta_d \approx a_d^{-1}$, where a_d is the particle size in microns.

Substituting $R = 3$ AU, and noting that there is no measurable sunward extension on the 1″ (∼1500 km) scale of the FWHM seeing, with $X_R \ll 1500$ km, we find $v_g \ll 45\beta_d^{1/2}$ m s^{-1}. With maximal $\beta_d = 1$, we find $v_g \ll 45$ m s^{-1}. For comparison, outgassing speeds in cometary dust comae are typically close to the sound speed in the sublimated gas. For R = 3 AU, this corresponds to $v_g \approx 400$ m s^{-1}. Thus, the absence of a measurable sunward extent to EP's coma is consistent with the slow ejection inferred from the narrow trail width.

4.3. *Finson-Probstein Modeling*

To advance beyond these order-of-magnitude considerations, we take recourse to Finson-Probstein type dust modeling (Finson & Probstein 1968). Our objective is to determine the grain size distribution and parameters of the ejection that are consistent with the width, surface brightness profile, and temporal evolution of the dust trail. We recognize from the outset that this is an underconstrained problem. Knowledge about size distribution, velocity versus size scaling, radiation pressure

factor β_d versus particle size, and time dependence of the dust emission are all lacking. Nevertheless, we can still use Finson-Probstein to limit the range of models that can fit the data and, so, understand something about the dust and the emission process.

We use Finson-Probstein modeling code provided by C. Lisse. It treats dust emission and its subsequent dynamical evolution under the influence of solar radiation and solar gravitation over a specified time period to produce a simulated dust trail. The models are focused on the observing geometry on 2002 September 7 (the night for which we obtained the best signal-to-noise ratio for the dust trail). We then take measurements of the simulated dust trails in the same way as for the actual data and make comparisons.

The dust emission can be described by the following simple model parameters:

Grain size.—Parameterized by β_d, the ratio of solar radiation pressure to solar gravitational acceleration;

Look-back time.—The time elapsed between an initial dust ejection event and the 2002 September 7 observations;

Ejection velocity.—Dependent on individual grain size, determined for meteoritic particles to roughly obey $v_g \propto \beta_d^{1/2}$ m s^{-1} (Whipple 1950, 1951).

The modeling code we use requires the use of a range of dust grain sizes. For simplicity and ease of detecting trends, test ranges of grain sizes are chosen to be relatively small, such that the smallest particles in each range have β_d-values 10 times larger than the β_d-values of the largest particles in each range. The β_d distribution for the smallest set of test particles is $0.1 < \beta_d < 1.0$ (1 μm $< a_d <$ 10 μm) and is $0.001 < \beta_d <$ 0.01 (100 μm $< a_d <$ 1000 μm) for the largest set. Each range of β_d-values is divided into 300 logarithmically spaced bins, which are each populated equally. The evolution of particles in the β_d bins is then computed to produce a series of syndynes (trajectories of dust grains of a single size), which are then integrated by the code to produce synchrones (locus of dust grains of all sizes emitted at a single time).

Dust grain sizes most likely obey a power-law size distribution, with large particles being less abundant than smaller ones. We nevertheless only consider a flat distribution to limit the scope of this simple analysis by minimizing the number of free parameters in consideration. This simplification has implications for the accuracy of our models but, as we discuss below, does not change our basic results.

To render trends more apparent, we further consider only single synchrones, representing impulsive emission events. In other words, each simulated trail represents a single emission burst (such as what might occur in the event of a collision with another asteroid) that is allowed to evolve into a dust trail over a certain time interval. This interval is what we call the look-back time, t. Prior to the initial emission event, no activity is assumed to have taken place.

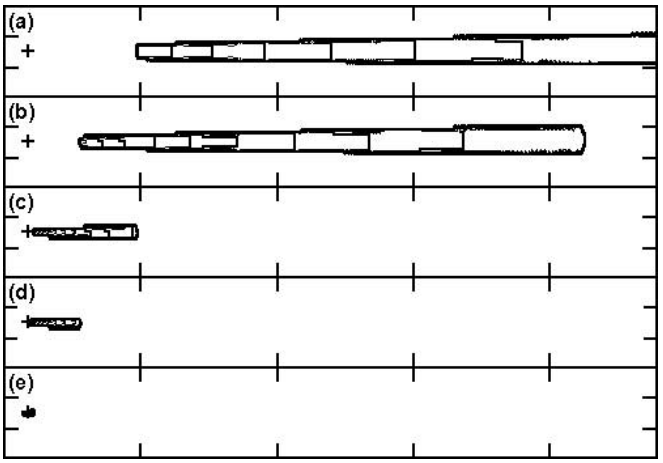

FIG. 11.—Contour plots of Finson-Probstein modeled dust trails for fixed look-back time (t = 30 days), fixed initial velocity law ($v_g = 2.0\beta_d^{1/2}$ m s^{-1}), and particle size ranges of (*a*) $0.1 < \beta_d < 1$ (1 μm $< a_d <$ 10 μm), (*b*) $0.05 < \beta_d < 0.5$ (2$\mu m < ad <$ 20μm), (*c*) $0.01 < \beta_d < 0.1$ (10 μm $< a_d <$ 100 μm), (*d*) $0.005 < \beta_d < 0.05$ (20 μm $< a_d <$ 200 μm), and (*e*) $0.001 < \beta_d < 0.01$ (100 μm $< a_d <$ 1000 μm). Individual fields of view shown are 0.′2 by 3.′5. Emission origins are at the far left of each frame and indicated by plus signs. Each contour interval represents 1/20 of full intensity range in logarithmic space.

There are several key notes we can make regarding our model synchrones:

1. Synchrone trail length is a strong function of the particle size. Small particles (characterized by large β_d) are quickly accelerated by solar radiation pressure and are pushed far from the nucleus in a short time. Meanwhile, large particles (small β_d) take longer to move away from the nucleus. This is illustrated in Figure 11, in which trail length is seen to shrink for increasing particle sizes for fixed look-back time and initial velocity distribution.

Trail lengths (in arcseconds on the sky) for our grid of synchrones are shown in Table 9. We note that, as expected, none of the trails for a 15 day look-back time appears plausible, as none reach the minimum observed length of 3′ (180″). By the same token, we can rule out the $0.001 < \beta_d < 0.01$ (100 μm$< a_d <$1000 μm) particle range for all times less than 90 days, as none of those trails reaches 3′ in length.

Thus, trail length provides a limit on the look-back time for a given particle size or, equivalently, a minimum particle size for a given look-back time. Unfortunately, it cannot uniquely determine both parameters simultaneously. As is evident from

TABLE 9
FINSON-PROBSTEIN MODEL RESULTS: TRAIL LENGTH

β_d Range	t = 15[a]	t = 30[a]	t = 45[a]	t = 60[a]	t = 75[a]	t = 90[a]	a_d Range[b]
$0.1 < \beta_d < 1$	75.2	>200	>200	>200	>200	>200	$10 > a_d > 1$
$0.05 < \beta_d < 0.5$	38.0	180.6	>200	>200	>200	>200	$20 > a_d > 2$
$0.01 < \beta_d < 0.1$	8.0	36.9	96.5	196.8	>200	>200	$100 > a_d > 10$
$0.005 < \beta_d < 0.05$	4.1	18.7	48.5	99.1	174.9	>200	$200 > a_d > 20$
$0.001 < \beta_d < 0.01$	1.0	4.1	10.0	20.3	35.6	57.3	$1000 > a_d > 100$

NOTE.—Listed is the distance of farthest extent of dust trail from the emission origin, in arcseconds.
[a] Look-back time in days.
[b] Approximate range of particle radii, a_d, corresponding to given β_d range, in microns.

TABLE 10
FINSON-PROBSTEIN MODEL RESULTS: RESULTS FOR DIFFERENT INITIAL VELOCITIES

Initial Velocity	Trail Width[a]	Trail Length[b]	Trail Detachment[c]
$v_g = 1.0\beta_d^{1/2}$	0.549	95.8	10.2
$v_g = 2.0\beta_d^{1/2}$	1.291	96.5	10.0
$v_g = 3.0\beta_d^{1/2}$	1.833	97.1	9.8
$v_g = 4.0\beta_d^{1/2}$	2.383	97.8	9.5
$v_g = 5.0\beta_d^{1/2}$	3.136	98.5	9.3

NOTE.—For β_d range held constant at $0.01 < \beta_d < 0.1$ (10 μm $< a_d <$ 100 μm) and look-back time held constant at $t = 45$ days. Data plotted in Fig. 14.

[a] Cross-sectional trail width (FWHM) in arcseconds, measured 30″ from emission origin.

[b] Distance of farthest extent of trail from emission origin, in arcseconds

[c] Distance between closest point of trail from emission origin, in arcseconds.

Table 10 and Figure 12, however, trail length is negligibly dependent on initial ejection velocity.

2. For the impulsive model used here and for all particle size distributions, the synchrone trail eventually detaches from the source and forms a gap, which should be observable upon emerging from the seeing disk of the comet nucleus. This effect is illustrated in Figure 13, where synchrone trails are seen to grow longer and separate farther from the emission source as time increases. This detachment distance (tabulated in Table 11) is dependent on particle size and look-back time but, like trail length, is negligibly dependent on initial ejection velocity (see Table 10 and Fig. 12). No trail separation was ever observed for EP, placing strong constraints on the particle size and look-back time.

3. We find that synchrone trail widths are primarily controlled by particle ejection velocities. The average observed trail width (FWHM) is about 1.″3 at 0.′5 from the nucleus for the September dust trail. Deconvolving this with the seeing to obtain an intrinsic width estimate and correlating with Figure 14 and Table 12, we find that $v_g \approx 1.5\beta_d^{1/2}$ m s^{-1}.

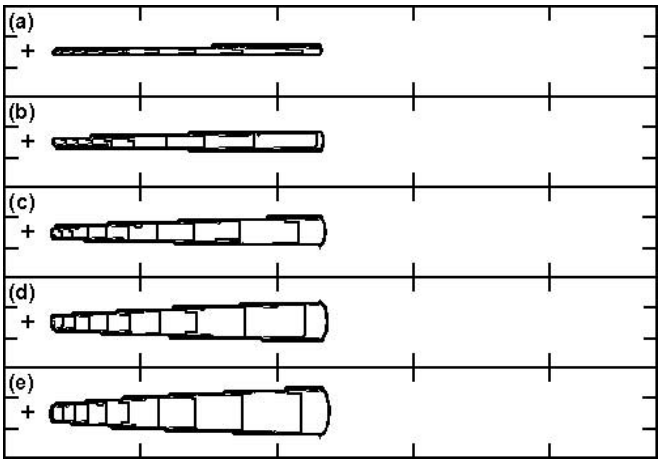

FIG. 12.—Contour plots of Finson-Probstein modeled dust trails for fixed particle size range ($0.01 < \beta_d < 0.1$; 10 μm $< a_d <$ 100 μm), fixed look-back time ($t = 45$ days), and initial velocity laws of (*a*) $v_g = 1.0\beta_d^{1/2}$ m s^{-1}, (*b*) $v_g = 2.0\beta_d^{1/2}$ m s^{-1}, (*c*) $v_g = 3.0\beta_d^{1/2}$ m s^{-1}, (*d*) $v_g = 4.0\beta_d^{1/2}$ m s^{-1}, and (*e*) $v_g = 5.0\beta_d^{1/2}$ m s^{-1}. Individual fields of view shown are 0.′2 by 3.′5. Emission origins are at the far left of each frame and indicated by plus signs. Each contour interval represents 1/20 of full intensity range in logarithmic space.

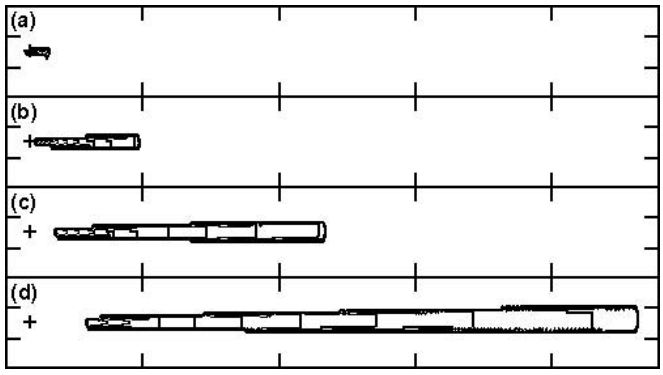

FIG. 13.—Contour plots of Finson-Probstein modeled dust trails for fixed particle size range ($0.01 < \beta_d < 0.1$; 10 μm $< a_d <$ 100 μm), fixed initial ejection velocity law ($v_g = 2.0\beta_d^{1/2}$ m s^{-1}), and look-back times of (*a*) $t = 15$ days, (*b*) $t = 30$ days, (*c*) $t = 45$ days, and (*d*) $t = 60$ days. Individual fields of view shown are 0.′2 by 3.′5. Emission origins are at the far left of each frame and indicated by plus signs. Each contour interval represents 1/20 of full intensity range in logarithmic space.

4. Finally, we investigate surface brightness profiles of our synchrones. Synchrone profiles for $0.05 < \beta_d < 0.5$ (2 μm $< a_d <$ 20 μm) and look-back times of 15, 30, 45, and 60 days are plotted in Figure 15. Soon after emission, all dust grains are found near the emission origin, resulting in a steep surface brightness profile. With time, however, small grains are preferentially pushed away by radiation pressure while large particles linger, flattening and extending the surface brightness profile. This result is consistent with our findings regarding the effect of particle sizes on trail length as a whole and detachment distance.

Another important aspect of Figure 15 is its demonstration of the inability of individual synchrones to fit observed 2002 September trail surface brightness data points. The individual synchrone profiles simply decline too rapidly with distance from emission origin. The solution thus must be a superposition of model trails, expanding the range of either emission times (combining different synchrones) or particle sizes (combining different syndynes).

Issues that we have already considered limit drastically the range of syndynes we have available. Apparent low ejection velocities of optically dominant dust particles, as implied by the lack of an observable sunward dust extension or coma-like dust halo around the nucleus and the narrow width of the dust trail, make extremely small particles unlikely to be optically significant. The relatively rapid disappearance of the trail in December, a matter of weeks after a detection in November, then excludes large particles ($\beta_d < 0.01$, or $a_d > 100$ μm), which can require many months to dissipate. Thus we are already limited to a narrow range of particle size possibilities.

We now recall that these synchrones are results of a flat distribution of particle sizes. If instead a more realistic power-law size distribution were used, in which more-abundant, smaller particles would not dissipate as quickly far from the nucleus, each synchrone's profile would not drop as steeply. Thus, with an appropriately scaled power-law distribution of particle sizes, these profiles could more closely approximate our observed surface brightness profiles. The overall length and detachment distance of the trails, however, only depend on the range limits themselves, not the distribution within a size range. The smallest particles will still form the farthest edge of the trail from the nucleus, while the largest particles will still form the closest edge. Thus, the need to avoid an

TABLE 11
FINSON-PROBSTEIN MODEL RESULTS: TRAIL DETACHMENT DISTANCE

β_d Range	$t = 15$[a]	$t = 30$[a]	$t = 45$[a]	$t = 60$[a]	$t = 75$[a]	$t = 90$[a]	a_d Range[b]
$0.1 < \beta_d < 1$	7.6	36.7	97.8	>200	>200	>200	$10 > a_d > 1$
$0.05 < \beta_d < 0.5$	3.9	18.5	49.4	102.0	181.5	>200	$20 > a_d > 2$
$0.01 < \beta_d < 0.1$	1.0	3.9	10.0	20.3	36.3	58.8	$100 > a_d > 10$
$0.005 < \beta_d < 0.05$	0.6	2.1	5.0	10.2	18.1	29.5	$200 > a_d > 20$
$0.001 < \beta_d < 0.01$	0.4	0.6	1.2	2.1	3.9	6.1	$1000 > a_d > 100$

NOTE.—Listed is the distance between closest point of dust trail from the emission origin, in arcseconds.
[a] Look-back time in days.
[b] Approximate range of particle radii, a_d, corresponding to given β_d range, in microns.

observable trail detachment between August and November while still producing a rapid dissipation between November and December leads us to conclude that changing the distribution of particle sizes within a given range would not fully account for our observations.

Therefore, we resort to combining synchrones, functionally approximating an extended emission event. The rough fit shown in Figure 16 is composed of 12 synchrones of arbitrarily varying intensity. A more cosmetically appealing fit might be obtained using a larger number of synchrones but would be no more physically enlightening. The necessity of using synchrone superposition to match the data already indicates that a long-duration emission event, such as what might result from solar sublimation of volatile surface materials (i.e., "outgassing"), is superior to a single emission burst, characteristic of an impact, for reproducing our observations.

More detailed numerical simulations of EP's dust production behavior are beyond the scope of this paper. From a limited number of simplified simulations and other physical considerations, however, we can still make the following conclusions:

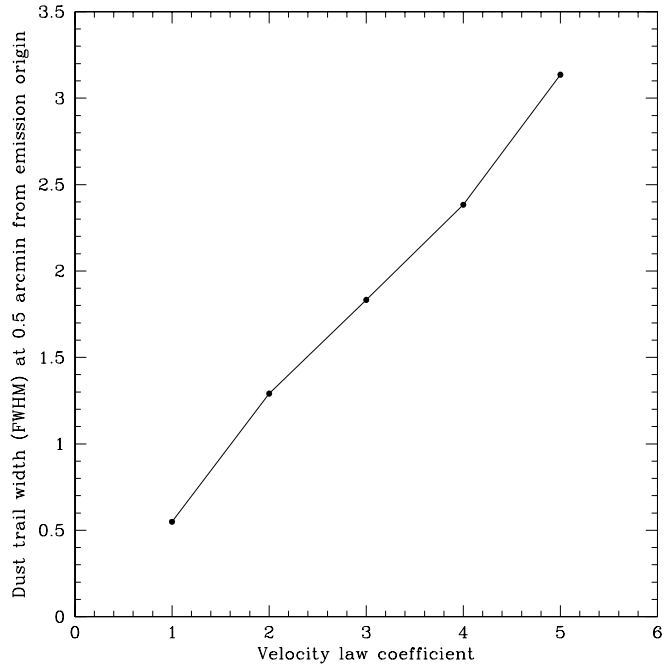

FIG. 14.—Intrinsic Finson-Probstein modeled trail widths (FWHM) in arcseconds as measured 0.″5 from emission origin for different initial velocities (images shown in Fig. 12). Initial velocities are defined by $v_g = k\beta_d^{1/2}$ m s^{-1}, where k is plotted on the x-axis. Particle size range ($0.01 < \beta_d < 0.1$; 10 μm $< a_d <$ 100 μm) and look-back time ($t = 45$ days) are held constant. Data tabulated in Table 10.

1. The particles carrying the bulk of the optical scattering cross section in the observed trail are in the 1–20 μm size range. Larger particles leave the vicinity of the nucleus so slowly that they cannot match the observed fading of the trail on a timescale of weeks between our November and December observations. Smaller particles should be ejected rapidly and produce a resolvable sunward coma extension, which is not observed. It is noteworthy that 2P/Encke, an object that is dynamically like EP, although closer to the Sun, also ejects large, slow particles that populate a trail (Reach et al. 2000; Lowry et al. 2003).

2. The emission must have continued until just shortly before our final observation of the trail in 2002 November. Otherwise, a resolvable gap should have opened between the dust and the nucleus, and none was observed.

3. The narrow trail width excludes large ejection velocities of the dust. Specifically, we estimate that $v_g \approx 1.5\beta_d^{1/2}$ m s^{-1}, which easily satisfies our analytical estimate based on equation (8).

Impulsive emission events (synchrones) cannot match the long undetached trail image or the surface brightness profile seen in 2002 September. The trail is also observed to persist between August and November, yet it disappears on a timescale of weeks between November and December. Therefore, we conclude that the trail must have been the result of an extended emission event lasting several months, a result consistent with cometary dust activity, but not with impact-generated dust activity.

5. DISCUSSION

Key features to be explained include

1. Continuous (nonimpulsive) ejection of $\sim$10 μm dust particles at very low velocities and rates;
2. Periods of dormancy following the 1996 and 2002 ejection events;
3. Unusually rapid rotation; and
4. An asteroid-like orbit.

5.1. *Gas-driven Mass Loss*

The ejection of dust particles could be caused by drag forces from gas produced thermally by the sublimation of near-surface ice. We calculate that the equilibrium sublimation rate of water ice exposed at the subsolar point (assuming albedo 0.05 and heliocentric distance of 3 AU) is $\sim 3 \times 10^{-5}$ kg m^{-2} s^{-1}. A trail production rate of about 10^{-2} to 10^{-3} kg s^{-1} (§ 4.1) would require areas of exposed ice ranging from a few tens to a few hundred square meters. The slow ejection of the particles suggests weak gas flow, as would be expected from water ice in sublimation beneath a thermally insulating mantle, or from an active area that is exposed obliquely to the Sun.

TABLE 12
FINSON-PROBSTEIN MODEL RESULTS: TRAIL WIDTH

β_d Range	$t = 15$[a]	$t = 30$[a]	$t = 45$[a]	$t = 60$[a]	$t = 75$[a]	$t = 90$[a]	a_d Range[b]
$0.1 < \beta_d < 1$	1.59	+	+	+	+	+	$10 > a_d > 1$
$0.05 < \beta_d < 0.5$	1.45	1.29	+	+	+	+	$20 > a_d > 2$
$0.01 < \beta_d < 0.1$	–	1.29	1.29	1.10	+	+	$100 > a_d > 10$
$0.005 < \beta_d < 0.05$	–	–	1.29	1.10	1.10	1.10	$200 > a_d > 20$
$0.001 < \beta_d < 0.01$	–	–	–	–	1.10	1.10	$1000 > a_d > 100$

NOTE.—Listed is the cross-sectional width (FWHM), in arcseconds, of the dust trail measured 0.″5 from the emission origin. Plus signs indicate that no measurement could be taken as the entire dust trail had already passed the 0.″5 reference mark. Minus signs indicate that no measurement could be taken as the dust trail had not yet arrived at the 0.″5 reference mark.

[a] Look-back time in days.

[b] Approximate range of particle radii, a_d, corresponding to given β_d range, in microns.

One prediction of the sublimation hypothesis is that the mass loss and trail production could, by analogy with the comets (e.g., Weissman 1987; Schleicher, Woodney, & Millis 2003), be seasonally modulated. In the case of EP, the heliocentric distance changes relatively little from perihelion to aphelion, but the effects of obliquity could nevertheless control the mass-loss rate as a function of position in the orbit. Is there evidence for this?

The 1996 dust trail was last observed on 1996 September 18 and had disappeared by 1997 September 29. Our new observations show a strong fading of the 2002 trail by 2002 December and complete disappearance by 2003 September. Unfortunately, the trail onset went unobserved both in the 1996 and 2002 seasons. Annual CCD monitoring of EP by H. Boehnhardt (2003, private communication) from 1997 through 2002 reveals no evidence of dust activity, though integration times were short. In particular, we note that Boehnhardt's observations on 2002 November 9–10 with the ESO Multi-Mode Instrument at the ESO 3.58 m New Technology Telescope were made only days after a successful deep-imaged 2002 November trail detection using the UH 2.2 m telescope reported in this paper. We therefore cannot definitively rule out any dust-emission activity in the intervening period between the dust trail's observed disappearance in 1997 September and our first observation in 2002 August. This, however, does not affect our primary result that EP activity is recurrent.

The 6 year interval between the observed trail apparitions is comparable to EP's 5.6 yr orbit period, suggesting that we may be witnessing a periodic ejection of matter in response to annual heating of an icy patch (possibly excavated by a recent impact) near the surface of EP. This simple hypothesis is compatible with the available observations (Tables 1 and 2) and provides a natural explanation for the intervening period of dormancy between 1996 and 2002, and it further admits a simple observational test over the next 5.6 yr.

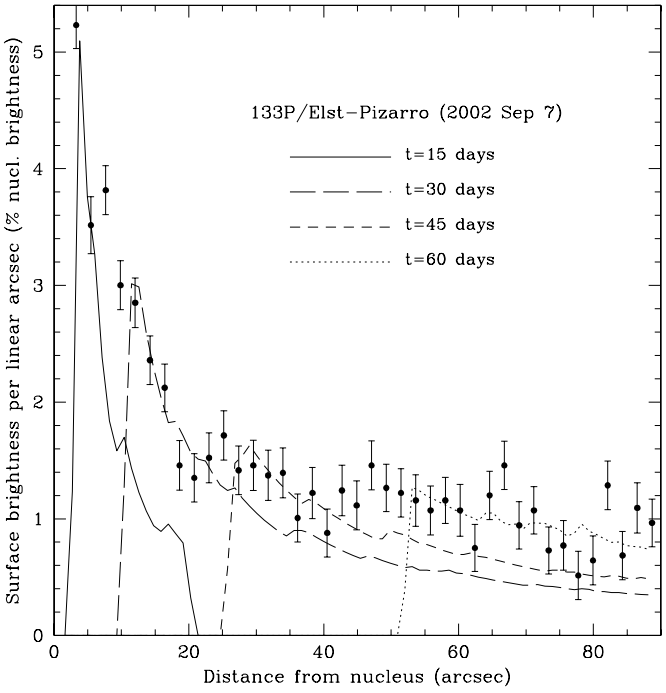

FIG. 15.—Sample fit of superposed profiles of model trails generated from an impulsive emission model to observed data points. For an average nucleus *R*-band magnitude of 19.7 on 2002 September 7, one trail surface brightness unit is equivalent to 24.7 mag per linear arcsecond. Individual profiles are arbitrarily scaled to approximate observed data.

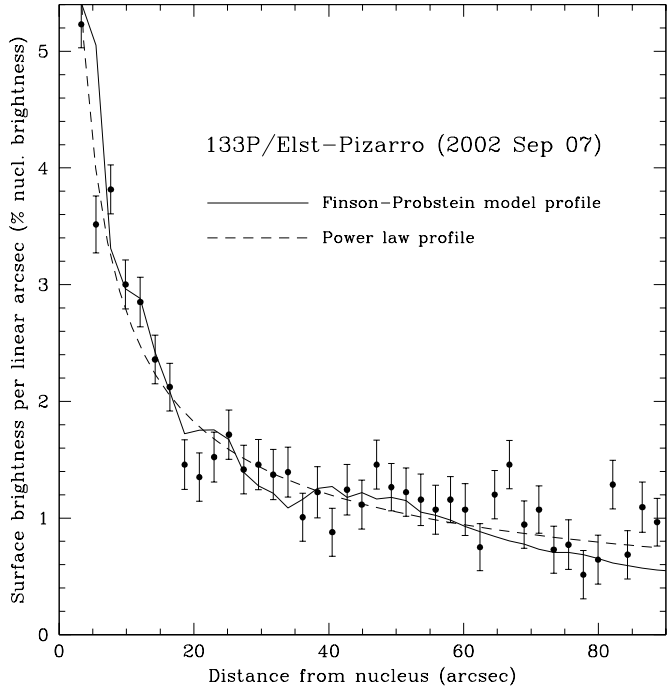

FIG. 16.—Surface brightness profile of a single model trail produced using 12 synchrones (impulsive events) of varying intensity occurring over 60 days, shown in comparison with surface brightness data measured from the 2002 September 7 dust-trail image. Also shown for reference is a power-law profile, varying as $\gamma^{-0.6}$, where γ is projected distance from the nucleus in arcseconds. For an average nucleus *R*-band magnitude of 19.7 on 2002 September 7, one unit of trail surface brightness is equivalent to 24.7 mag per linear arcsecond.

If the 1996 and 2002 emission events are consequences of seasonal insolation variation, the area of exposed surface volatiles must be located near one of the rotational poles of the nucleus and the object's obliquity must be nonzero. This volatile region would then only receive enough solar radiation to become active when the near pole tilts toward the Sun, that is, during that hemisphere's "summer." Elsewhere in the orbit, the volatile region would not receive enough solar heating to sublimate. Assuming minimal non–principal-axis rotation and minimal precession of the principal rotational axis over a small number of orbits, recurrence of seasonal activity should be consistent with EP's orbit period of 5.6 yr. A strong trail should next appear in late 2007 and dissipate by mid-to-late 2008. Observations of EP around this time will help to confirm or refute this hypothesis. We note that the appearance of a trail before this time will not explicitly exclude our hypothesis. Instead, there may simply be more than one active area on EP's surface. The nonappearance of a trail in late 2007 would, however, eliminate the possibility that dust emission from EP is seasonally modulated and cast doubt on the sublimation hypothesis itself.

5.2. *Non–Gas-driven Mass Loss*

Dust could be ejected by a process other than gas drag. Tóth (2000) and others have suggested that impacts with other asteroids or their associated debris could be responsible. The persistent nature of the dust emission in both 1996 and 2002 requires the invocation of more complex scenarios than a simple single impact, however. Then there is the matter of the activity's recurrence. Given the already low likelihood of the complex impact scenarios that have been proposed, the repetition of similar behavior after only about 6 years further increases the implausibility of any impact-driven mechanism as an explanation for EP's behavior.

We note that a mechanism exists by which a single emission episode might appear to be two separate events. A neck-line structure consists of ejected cometary dust grains that collapse back onto the comet's orbit plane 180° away in true anomaly, ν, from their respective ejection points (Pansecchi, Fulle, & Sedmak 1987). Seen edgewise on the sky, this relic of past emission could create the illusion of current activity when in fact none exists. Neck-line structures have been observed for comets Bennett 1970 II, (Pansecchi et al. 1987), 1P/Halley (Fulle 1987), C/1910 I (Pansecchi & Fulle 1990), and 2P/Encke (Epifani et al. 2001), among others. Observation of a neck-line structure requires that Earth be at a low cometocentric latitude (which was the case during our 2002 EP observations) and that the comet be observed at $\Delta\nu = 180°$ from the point of the initial dust emission. The 1996 emission time estimated by Sekanina (Pravec & Sekanina 1996) and our 2002 observations, however, are separated by only $\Delta\nu \lesssim 80°$, ruling out the possibility that the dust trail we observe in 2002 is simply a long-lived neck-line structure resulting from a single 1996 impact event.

Levitation of dust by electrostatic charging at the terminator has been observed in situ on the Moon (e.g., De & Criswell 1977), while Mendis et al. (1981) and Lee (1996) have suggested that this phenomenon may also occur on comets and asteroids. On the Moon, dust is launched from the surface at about 1 m s^{-1} and falls back to the surface under lunar gravity. There is no net loss of dust. On EP, the low escape velocity (also $\sim$1 m s^{-1}) would allow electrostatically levitated dust to be lost to interplanetary space, perhaps producing the trail. One obvious difficulty with this hypothesis is that the supply of mobile dust on the surface of EP would be quickly depleted, with no obvious source of fresh dust to replenish the trail. A second problem is that the effectiveness of electrostatic levitation is diminished on a rapid rotator such as EP as a result of the shorter time that any given area continuously spends in sunlight, because less photoelectric charge can be accumulated. Still a third problem is that it is not clear how electrostatic levitation, whose efficacy is independent of heliocentric distance, could produce the intermittent ejection that we observe, with a period of inactivity between bursts of activity that last, at minimum, several months each. Lastly, EP should not be the only asteroid observed with a trail. If dust emission is caused by a process as universal as electrostatic charging, all small asteroids should be accompanied by a trail of electrostatically levitated and ejected dust particles. This is evidently not the case. Given these inconsistencies, we believe that electrostatic ejection is not a likely mechanism for EP's dust emission.

A similar supply problem would apply if EP were an asteroid losing mass from its surface because it rotates on the verge of centripetal instability. The natural consequence of spin-up to instability is a temporary shedding of mass followed by settling into a state just below instability. One would expect the ejection of mass and angular momentum to be impulsive and followed by long periods of stability, unless the nucleus is somehow continually pushed back toward the rotational limit.

Could EP be held at the brink of rotational instability by torques due to radiation forces? The Yarkovsky-O'Keefe-Radzievsky-Paddack (YORP) effect is a torque imparted by the asymmetric absorption of solar radiation and its subsequent thermal reemission as infrared radiation. For $R < 5$ km asteroids in the inner solar system, the YORP spin-up timescale is shorter than the collisional spin-up timescale. Rubincam (2000) estimates that the timescale for the YORP effect to significantly alter the spin state of a kilometer-scale body ranges from 10^6 to 10^8 yr, depending on the shape, size, and location of the body. Vokrouhlický & Čapek (2002) report that a Themis-family asteroid with an initial rotational period of $P_{\rm rot} \approx 6$ hr can spin up to as fast as $P_{\rm rot} \approx 4$ hr after about 25–35 Myr of YORP evolution before spinning down to $P_{\rm rot} > 100$ hr after 100 Myr. Thus, the YORP effect could be a driver of EP's spin-state evolution but would not obviously leave EP with a rapid spin.

While we cannot absolutely rule out the hypothesis that EP is a refractory body, devoid of any volatile material, the contrived circumstances that must be invoked to explain its recurring trail lead us to believe that this interpretation is unlikely. Among various technical issues, the most significant difficulties arise in trying to explain the intermittence, recurrence, and long duration of each of EP's observed dust-emission events. We prefer the simpler explanation that EP's dust emission is sublimation-driven, meaning that EP itself, by classical physical and observational definitions, is a comet among the asteroids.

5.3. *The Nature and Origin of 133P/Elst-Pizarro*

EP unambiguously satisfies the practical, observational definition of a comet. We naturally must now ask what the origin of this object might be. If, as we believe, the mass loss from EP reflects sublimation of near-surface ice, then we are faced with two basic possibilities for the origin of this object.

Either EP is a JFC whose orbit has evolved into the region of the main asteroid belt, or it is a bona fide asteroid that contains substantial near-surface ice.

5.3.1. *The Comet Hypothesis*

The most difficult observation for the comet hypothesis to explain is EP's asteroid-like orbit, which, unlike most JFC orbits, is largely decoupled from Jupiter. Similar orbits are not produced with significant frequency in current models of the dynamics of JFCs. Decoupling from Jupiter is thought to require perturbations by the terrestrial planets and particularly by nongravitational forces such as asymmetric outgassing. Models including the latter have not been explored in great detail. Ipatov & Hahn (1997) analyzed the long-term dynamical evolution of EP's current orbit under gravitational influences and found it to be quite stable, implying that evolution of a JFC-type object onto such an orbit would be a rare event. Ipatov (2004, private communication) suggested, however, that EP's orbit could have been less stable in the past and only made more stable later by nongravitational influences. Fernández et al. (2002) were able to gravitationally evolve a sample JFC (D/Pigott in their simulations) into an orbit with a 2:1 mean motion resonance with Jupiter, mimicking EP's orbit, but could not find a purely gravitational solution for reproducing EP's low inclination ($i = 1.^\circ4$, vs. $i \sim 25^\circ$–30° for an evolved D/Pigott). The dynamical problems in understanding EP are, to some extent, shared by 2P/Encke, whose cometary nature is not in question.

Despite elements of doubt that it casts, the extremely low likelihood of a JFC evolving into a main-belt orbit actually favors parts of the comet hypothesis. We recall that key characteristics of EP include its apparent uniqueness among other asteroids and a currently low activity level. Given the difficulty of such a drastic dynamical transition, it is entirely natural that only one object (EP) has been observed thus far to have completed the transition. If a large expenditure of volatile material over the course of several perihelion passages is required to effect such a transition, most JFCs undergoing similar evolution might simply exhaust their volatile content or disintegrate by the time they reach the asteroid belt, rendering them observationally undetectable as comets. Under this hypothesis, EP is simply a particularly robust comet whose volatile content has almost, but not completely, been exhausted by a near-lifetime of gas-driven dynamical evolution.

We believe that the numerical exploration of the dynamical decoupling of JFCs from Jupiter under the action of outgassing forces is in need of urgent attention. Unfortunately, we expect an exact determination of EP's evolutionary history to be difficult to achieve, since EP's original orbit and activity level are likely much different from what we currently see and thus difficult to properly constrain. As seen in simulations performed by Fernández et al. (2002), gravitational perturbations alone can produce large orbital deviations: D/Pigott migrates from a perihelion distance of $q \sim 1$ AU to one as high as $q \sim 3$ AU. Outgassing is of course more vigorous at smaller heliocentric distances and so may have been a much stronger influence early on in EP's dynamical history than is apparent today. As such, we feel that current understanding of the long-term dynamical consequences of nongravitational forces is inadequate and cannot be used to rule out the hypothesis that EP may be a highly dynamically evolved JFC.

The density we derived earlier for EP is larger than the nominal densities associated with other cometary nuclei. However, there are no direct measurements of the density of any nucleus. The best case is that of D/Shoemaker-Levy 9 ($\rho_n \sim 600$ kg m^{-3}), whose density was inferred from analysis of its tidal disruption by Jupiter (Asphaug & Benz 1996). Densities for other comet nuclei should be regarded as effectively unknown. Thus, there is no fundamental reason to preclude the existence of a comet nucleus with $\rho_n \geq 1300$ kg m^{-3} as inferred here for EP.

The comet hypothesis might also account for EP's rapid rotation. The timescale for nucleus spin-up via outgassing torques is potentially short and scales, for a given mass-loss rate, with the fourth power of the nucleus radius (Samarasinha et al. 1986; Jewitt 1992). Spin-up by outgassing is insignificant given the current, low rates of mass loss but could have been rapid if the mantling of EP were smaller in the past than now. For example, for an $r \sim 2$ km body at $R = 3$ AU, the spin-up timescale for an active nucleus is comparable to the orbit period and 3 orders of magnitude less than the timescale for the depletion of volatiles from the nucleus by sublimation (see Fig. 2 of Jewitt 1999). Thus, outgassing torques could have induced EP's rapid spin while leaving behind buried volatiles to drive the current mass loss. In this case, the EP dust trail consists of material ejected by the last gasps of outgassing produced by sublimating volatile ices. One obvious possibility is that dust leaves the nucleus of EP aided by the substantial centripetal acceleration provided by the rapid rotation, the latter itself a product of past outgassing.

5.3.2. *The Icy-Asteroid Hypothesis*

The second possibility is that EP was formed and has remained for the age of the solar system at or near its current main-belt location but nevertheless contains an ice component. The possibility that water ice might be present in main-belt asteroids has been suggested (Jones et al. 1990; Barucci, Fulchignoni, & Lazzarin 1996 and references within), but to date, no direct physical evidence has come to light. EP's behavior may have changed this.

Could ice survive in EP? The timescale for heat to conduct from the surface of EP to the core is given by r_e^2/κ, where r_e is the effective radius and κ is the thermal diffusivity of the material of which EP is made. With $r_e \sim 2$ km (§ 3.1) and $\kappa = 10^{-6}$ m^2 s^{-1} as appropriate for a rocky body, we estimate that the thermal conduction timescale is on the order of 10^5 yr. This is long compared with the ~6 yr orbit period but short compared with the likely age of the Themis family, estimated between a few hundred million years and 2 Gyr (Marzari, Davis, & Vanzani 1995). Therefore, we assume that EP has thermally equilibrated to the average temperature of a corresponding graybody moving around the Sun in the orbit of EP. This temperature is near 160 K. At this temperature, water ice does not sublimate immediately, but it nonetheless remains unstable over geologically long timescales. The rate of water ice sublimation at 160 K is about 10^{-7} kg m^{-2} s^{-1}, corresponding to recession of a sublimating ice surface (with $\rho = 1000$ kg m^{-3}) at the rate of about 10^{-10} m s^{-1}.

At this recession rate, a dark sphere of ice with $r = 2$ km could survive for only ~10^6 yr in the orbit of EP. However, sublimation on comets is normally throttled by a refractory surface mantle (Whipple 1950), and so the same might occur on an icy, outgassing asteroid as a result of the loss of volatiles from the upper layers. EP could be losing mass through a hole in the mantle, perhaps resulting from a past impact, but the bulk of the ice in the interior could survive essentially

indefinitely. Fanale & Salvail (1989) present detailed models showing that water ice could be stable over 4.5 Gyr on Ceres at depths of only a few to a few tens of meters, consistent with the inference that subsurface ice could be stable at shallow depths in the more distant EP. Then, given the enhanced probability of collisions among Themis-family asteroids (Farinella & Davis 1992), it is reasonable to expect that EP could have been struck recently and "activated," causing it to betray its icy nature.

R. P. Binzel (2003, private communication) has suggested the term "activated asteroid" for such an object. This scenario remains consistent with the possibility of seasonal modulation of EP's activity, since an impact would naturally provide the needed exposed patch of volatile material. An obvious consequence of this hypothesis is that the outer asteroid belt could be host to many more ice-laden bodies that have thus far escaped detection because of the rarity of activation events and the transience of emission activity even after an activation has taken place. A deep survey of outer main-belt asteroids in high collisional environments, such as the Themis family region in which EP itself resides, might turn up more activated asteroids and represents a natural avenue for further investigation. This, along with more realistic simulation of the orbital evolution of outgassing JFCs, would seem to be the next logical step in seeking to uncover EP's true nature.

6. SUMMARY

Observations of 133P/Elst-Pizarro (EP) were made on several occasions during 2002 and 2003. Results concerning the nucleus include the following:

1. Time-resolved photometry of the nucleus shows a double-peaked period of $P_{\rm rot} = 3.471 \pm 0.001$ hr, which we take as the rotational period of an aspherical body. The photometric range of $\Delta m_R = 0.40 \pm 0.05$ mag corresponds to a lower limit to the axis ratio (due to possible projection effects) of $a/b = 1.45 \pm 0.07$.

2. The absolute R-band magnitude, rotationally averaged and normalized to zero phase angle and unit heliocentric and geocentric distances, is $H_R = 15.3 \pm 0.1$. Assuming an elliptical cross section, geometric albedo $p_R = 0.04$, and axis ratio $a/b = 1.45$, we estimate nucleus semiaxes of $a \sim 3.0$ km and $b \sim 2.1$ km.

3. The rotationally averaged apparent magnitude of the EP nucleus varies with phase angle, α, in the range $7\overset{\circ}{.}5 \leq \alpha \leq 18\overset{\circ}{.}7$ with a linear phase-darkening coefficient of $\beta = 0.044 \pm 0.007$ mag deg^{-1}. This is consistent with β-values measured for other known cometary nuclei and is suggestive of, but does not require, a low-albedo surface.

4. Optical colors measured for the EP nucleus ($B-V = 0.69 \pm 0.02$, $V-R = 0.42 \pm 0.03$, $R-I = 0.27 \pm 0.03$) are approximately solar and comparable both to other comets and to the C-type asteroids.

5. EP must have a bulk density of $\rho_n \geq 1300$ kg m^{-3} to not be in a state of internal tensile stress.

Results concerning the dust trail include the following:

1. A long, narrow dust trail is present. At its brightest, it is seen extending almost $3\overset{\prime}{.}5$ (about 4.5×10^5 km in the plane of the sky) from the EP nucleus, with an intrinsic (seeing-corrected) width of $0\overset{\prime\prime}{.}9$ (1200 km in the plane of the sky). No coma is detected at any time during our observations.

2. The dust trail fades by a factor of about 3 from 2002 August to 2002 December and is undetectable by 2003 September. The fading is due to a real loss of particles and is not a geometric effect.

3. Finson-Probstein type models of the observed dust trail suggest that dust particles approximately 1–20 μm in size are continuously released with low ejection velocities ($v_g \approx 1.5$ m s^{-1}) from the EP nucleus over a minimum period of 5 months from 2002 July through November.

Conclusions concerning the nature of EP include the following:

1. The persistence of the EP dust trail over many months in both 1996 and 2002 is inconsistent with dust emission being triggered by a simple impact.

2. The leading hypothesis for the EP dust trail in 1996 (collisions from a swarm of impactors) is rendered implausible in light of the reemergence of the trail in 2002. Instead, the dust is more likely to be ejected from the nucleus by drag forces caused by gas liberated from EP by sublimation of near-surface ice.

3. By the classical observational definition, EP is an active comet. If our conclusion regarding the nature of EP's dust emission is correct, as an ice-containing body EP also satisfies the classical physical definition of a comet. Dynamically, however, it appears to be an unremarkable member of the main asteroid belt and of the Themis collisional family in particular.

4. We divide hypotheses for EP's mass loss into gas-driven and non–gas-driven categories. Gas-driven mass-loss hypotheses invoke near-surface ice that sublimates, releasing gas that blows dust particles out of the nucleus of EP in classical cometary fashion. Non–gas-driven mass-loss hypotheses invoke the rapid rotation of EP and, possibly, electrostatic charging and levitation of surface dust to populate the trail. The variable and repetitive nature of the mass loss is expected in sublimation hypotheses (the two known trail apparitions occur near perihelion and about one orbit period apart) but is less naturally explained by rotational instability or electrostatic ejection.

5. Given its cometary nature, EP could be a JFC that has evolved into an asteroid-like orbit via planetary gravitational scattering and nongravitational forces due to outgassing. Its observed mass loss and other physical properties are then easily explained, though its apparent membership in the Themis family would necessarily be simply coincidental. The main weakness of this hypothesis is that the dynamical path from a comet orbit to an asteroid orbit is not well established. This may be because of the general lack of emphasis on nongravitational forces in most current dynamical evolution models, suggesting that more work in this area would be valuable.

6. Alternatively, EP could be a true Themis family member upon which subsurface ice has been recently exposed, perhaps by an impact. EP would then still blur the asteroid-comet boundary by showing that small main-belt asteroids can preserve ice over astronomically long timescales. Such a scenario would greatly complicate the determination of source regions for near-Earth objects, since the presence of significant ice in a body could no longer be considered a diagnostic of origin in the outer solar system and not the main asteroid belt. Intriguingly, this scenario also potentially implicates main-belt asteroids (and not just JFCs and HFCs) in the early delivery of organic volatiles to the terrestrial planets.

We thank Scott Sheppard for providing telescope time, IDL help, and helpful comments on this manuscript. We also

thank Karen Meech for providing telescope time, as well as University of Hawaii telescope operators John Dvorak, Andrew Pickles, Paul de Grood, and Ian Renaud-Kim, and Keck Observatory observing assistant Gary Punawai, for their assistance. We also acknowledge Marc Buie for providing phase dispersion minimization code, Casey Lisse for providing Finson-Probstein modeling code, the JPL Solar System Dynamics group for their useful Web-based ephemeris generator, ''Horizons,'' and Richard Binzel and an anonymous referee for useful suggestions for improving this paper. This work was supported by a grant to D. C. J. from NASA.

REFERENCES

Asphaug, E., & Benz, W. 1996, Icarus, 121, 225
Barucci, M. A., Fulchignoni, M., & Lazzarin, M. 1996, Planet. Space Sci., 44, 1047
Belskaya, I. N., & Shevchenko, V. G. 2000, Icarus, 147, 94
Boehnhardt, H., Schulz, R., Tozzi, G. P., Rauer, H., & Sekanina, Z. 1996, IAU Circ. 6495
Boehnhardt, H., Sekanina, Z., Fiedler, A., Rauer, H., Schulz, R., & Tozzi, G. 1998, Highlights Astron., 11A, 233
Bottke, W. F., Morbidelli, A., Jedicke, R., Petit, J.-M., Levison, H. F., Michel, P., & Metcalfe, T. S. 2002, Icarus, 156, 399
Bowell, E., Hapke, B., Domingue, D., Lumme, K., Peltoniemi, J., & Harris, A. W. 1989, in Asteroids II, ed. R. P. Binzel, T. Gehrels, & M. S. Matthews (Tucson: Univ. Arizona Press), 524
Bowell, E., Skiff, B. A., West, R. M., Heyer, H.-H., Quebatte, J., Marsden, B. G., & Bus, S. J. 1992, IAU Circ. 5585
Burns, J. A., Lamy, P. L., & Soter, S. 1979, Icarus, 40, 1
De, B. R., & Criswell, D. R. 1977, J. Geophys. Res., 82, 999
Delahodde, C. E., Meech, K. J., Hainaut, O. R., & Dotto, E. 2001, A&A, 376, 672
Elst, E. W., et al. 1996, IAU Circ. 6456
Epifani, E., et al. 2001, Icarus, 149, 339
Fanale, F. P., & Salvail, J. R. 1989, Icarus, 82, 97
Farinella, P., & Davis, D. R. 1992, Icarus, 97, 111
Fernández, J. A., Gallardo, T., & Brunini, A. 2002, Icarus, 159, 358
Fernández, Y. R., Jewitt, D. C., & Sheppard, S. S. 2001, ApJ, 553, L197
Fernández, Y. R., McFadden, L.-A., Lisse, C. M., Helin, E. F., & Chamberlin, A. B. 1997, Icarus, 128, 114
Finson, M. L., & Probstein, R. F. 1968, ApJ, 154, 327
Fulle, M. 1987, A&A, 181, L13
Hammergren, M. 1996, BAAS, 28, 1299
Hanner, M. S. 1981, Icarus, 47, 342
Hardorp, J. 1980, A&A, 88, 334
Harris, A. W. 1996, in Lunar and Planetary Science XXVII (Houston: Lunar Planet. Inst.), 493
Harris, N. W., & Bailey, M. E. 1998, MNRAS, 297, 1227
Hartmann, W. K., Cruikshank, D. P., & Degewij, J. 1982, Icarus, 52, 377
Hartmann, W. K., Tholen, D. J., & Cruikshank, D. P. 1987, Icarus, 69, 33
Hartmann, W. K., Tholen, D. J., Meech, K. J., & Cruikshank, D. P. 1990, Icarus, 83, 1
Ipatov, S. I., & Hahn, G. J. 1997, in Lunar and Planetary Science XXVIII (Houston: Lunar Planet. Inst.), 619
Jewitt, D. 1992, in Observations and Physical Properties of Small Solar System Bodies, ed. A. Brahic, J.-C. Gérard, & J. Surdej (Liège: Inst. d'Astrophys., Univ. Liège), 85
———. 1996, Earth Moon Planets, 72, 185
———. 1999, Earth Moon Planets, 79, 35
Jewitt, D., & Luu, J. 1989, AJ, 97, 1766
Jewitt, D., Sheppard, S., & Fernández, Y. 2003, AJ, 125, 3366
Jewitt, D. C. 2002, AJ, 123, 1039
Jewitt, D. C., & Meech, K. J. 1987, ApJ, 317, 992
Jones, T. D., Lebofsky, L. A., Lewis, J. S., & Marley, M. S. 1990, Icarus, 88, 172
Jorda, L., & Gutiérrez, P. 2002, Earth Moon Planets, 89, 135
Kresák, L. 1980, Moon Planets, 22, 83
Landolt, A. U. 1992, AJ, 104, 340
Lee, P. 1996, Icarus, 124, 181
Lowry, S. C., Weissman, P. R., Sykes, M. V., & Reach, W. T. 2003, in Lunar and Planetary Science XXXIV (Houston: Lunar Planet. Inst.), No. 2056
Luu, J. X., & Jewitt, D. C. 1992a, AJ, 104, 2243
———. 1992b, Icarus, 97, 276
Marsden, B. G. 1996, IAU Circ. 6457
Marzari, F., Davis, D., & Vanzani, V. 1995, Icarus, 113, 168
McNaught, R. H., Hawkins, M. R. S., Marsden, B. G., Boehnhardt, H., Sekanina, Z., & Offutt, W. 1996, IAU Circ. 6473
Mendis, D. A., Hill, J. R., Houpis, H. L. F., & Whipple, E. C., Jr. 1981, ApJ, 249, 787
Offutt, W., Marsden, B. G., & Boehnhardt, H. 1997, Minor Planet. Electron. Circ., No. 1997-T03
Oke, J. B., et al. 1995, PASP, 107, 375
Pansecchi, L., & Fulle, M. 1990, A&A, 239, 369
Pansecchi, L., Fulle, M., & Sedmak, G. 1987, A&A, 176, 358 (erratum 205, 367 [1988])
Pravec, P., Hergenrother, C., Whiteley, R., Šarounová, L., Kušnirák, P., & Wolf, M. 2000, Icarus, 147, 477
Pravec, P., & Sekanina, Z. 1996, IAU Circ. 6459
Pravec, P., Wolf, M., & Šarounová, L. 1998, Icarus, 136, 124
Press, W. H., Teukolsky, S. A., Vetterling, W. T., & Flannery, B. P. 1992, Numerical Recipes in C (2nd ed.; Cambridge: Cambridge Univ. Press)
Reach, W. T., Sykes, M. V., Lien, D., & Davies, J. K. 2000, Icarus, 148, 80
Rubincam, D. P. 2000, Icarus, 148, 2
Russell, H. N. 1916, ApJ, 43, 173
Samarasinha, N. H., A'Hearn, M. F., Hoban, S., & Klinglesmith, D. A., III. 1986, in Proc. 20th ESLAB Symp. on the Exploration of Halley's Comet, Vol. 1, Plasma and Gas, ed. B. Battrick (Paris: ESA), 487
Schleicher, D. G., Woodney, L. M., & Millis, R. L. 2003, Icarus, 162, 415
Stellingwerf, R. F. 1978, ApJ, 224, 953
Tóth, I. 2000, A&A, 360, 375
Vaghi, S. 1973, A&A, 24, 107
Vokrouhlický, D., & Čapek, D. 2002, Icarus, 159, 449
Weissman, P. R. 1987, A&A, 187, 873
Whipple, F. L. 1950, ApJ, 111, 375
———. 1951, ApJ, 113, 464
Whiteley, R. J., Tholen, D. J., & Hergenrother, C. W. 2002, Icarus, 157, 139
Williams, I. P., & Wu, Z. 1993, MNRAS, 262, 231
Zappalà, V., Cellino, A., Farinella, P., & Knežević, Z. 1990, AJ, 100, 2030
Zellner, B., Tholen, D. J., & Tedesco, E. F. 1985, Icarus, 61, 355